



Quantitative structure–activity relationship studies of *threo*-methylphenidate analogs

Milind Misra^{a,†}, Qing Shi^b, Xiacong Ye^b, Ewa Gruszecka-Kowalik^b, Wei Bu^b, Zhanzhu Liu^b, Margaret M. Schweri^c, Howard M. Deutsch^b, Carol A. Venanzi^{a,*}

^a Department of Chemistry and Environmental Science, New Jersey Institute of Technology, Newark, NJ 07102, USA

^b School of Chemistry and Biochemistry, Georgia Institute of Technology, Atlanta, GA 30332-0400, USA

^c Retired from Mercer University School of Medicine, Macon, GA 31207-0001, USA

ARTICLE INFO

Article history:

Received 11 June 2010

Revised 8 August 2010

Accepted 14 August 2010

Available online 19 August 2010

Keywords:

Molecular descriptors

Dopamine transporter

Methylphenidate

Comparative molecular field analysis

ABSTRACT

Complementary two-dimensional (2D) and three-dimensional (3D) Quantitative Structure–Activity Relationship (QSAR) techniques were used to derive a preliminary model for the dopamine transporter (DAT) binding affinity of 80 racemic *threo*-methylphenidate (MP) analogs. A novel approach based on using the atom-level E-state indices of the 14 common scaffold atoms in a sphere exclusion protocol was used to identify a test set for 2D- and 3D-QSAR model validation. Comparative Molecular Field Analysis (CoMFA) contour maps based on the structure–activity data of the training set indicate that the 2' position of the phenyl ring cannot tolerate much steric bulk and that addition of electron-withdrawing groups to the 3' or 4' positions of the phenyl ring leads to improved DAT binding affinity. In particular, the optimal substituents were found to be those whose bulk is mainly in the plane of the phenyl ring. Substituents with significant bulk above or below the plane of the ring led to decreased binding affinity. Suggested alterations to be explored in the design of new compounds are the placement at the 3' and 4' position of the phenyl ring of electron-withdrawing groups that lie chiefly in the plane of the ring, for example, halogen substituents on the 3',4'-benzo analog, **79**. A complementary 2D-QSAR approach—partial least squares analysis using a reduced set of Molconn-Z descriptors—supports the CoMFA structure–activity interpretation that phenyl ring substitution is a major determinant of DAT binding affinity. The potential usefulness of the CoMFA models was demonstrated by the prediction of the binding affinity of methyl 2-(naphthalen-1-yl)-2-(piperidin-2-yl)acetate, an analog not in the original data set, to be in good agreement with the experimental value.

© 2010 Elsevier Ltd. All rights reserved.

1. Introduction

Cocaine binds to the dopamine transporter (DAT) in the brain and is believed to produce its euphoric and addictive effects by inhibiting the reuptake of synaptic dopamine into presynaptic neurons.^{1,2} Structure–activity relationship (SAR) studies for several classes of dopamine reuptake inhibitors have been reviewed.^{3–6} *threo*-Methylphenidate (MP) and its analogs comprise one such class that has been studied as possible cocaine abuse therapeutics. Although both MP and cocaine are potent inhibitors of dopamine transport, they have markedly different effects at several other neuronal sites. MP has significant inhibitory activity at the norepinephrine transporter and virtually none at the serotonin transporter, while cocaine has significant activity at the serotonin

transporter and less at the norepinephrine transporter.^{7,8} Unlike cocaine,⁹ MP is not a sodium channel blocker and hence would not be expected to slow neuronal conduction. Perhaps because of these important differences, MP has found use as an orally-administered medication for the long-term treatment of children with attention deficit hyperactivity disorder.

The accumulated experience with MP in a large pediatric population, coupled with a relatively low incidence of serious side effects and little evidence of abuse potential, have generated considerable interest in MP and its analogs as potential pharmacotherapies for cocaine abuse. The wide range of MP SAR studies produced by ourselves and others^{7,8,10–23} provides a large amount of data for pharmacophore modeling.²⁴ However, although the amino acid sequence of the DAT has been identified,²⁵ its three-dimensional structure is not known, necessitating a ligand-based rather than structure-based modeling approach. As a first step in this direction, we have recently carried out an exhaustive conformational analysis²⁶ of neutral (nMP) and protonated (pMP) methylphenidate, comparing their potential energy surfaces in various

* Corresponding author. Tel./fax: +1 (973) 596 3596.

E-mail address: carol.a.venanzi@njit.edu (C.A. Venanzi).

† Present address: Multiscale Dynamic Materials Modeling Department, Sandia National Laboratories, Albuquerque, NM 87185-1322, USA.

molecular mechanics, molecular orbital, and solvation models to each other and to rotationally restricted MP analogs.⁸ The present work takes this computer modeling a step further by using complementary two-dimensional (2D) and three-dimensional (3D) Quantitative Structure–Activity Relationship (QSAR) approaches to generate a preliminary model for the DAT binding of 80 MP analogs. The simple models produced by these studies identified phenyl ring modification as a major determinant of DAT binding affinity. This paves the way for our future comprehensive 3D-QSAR studies of MP analogs with only phenyl ring substitutions. Previously, 2D-^{27–29} and 3D-QSAR^{30–42} studies have been carried out on other dopamine reuptake inhibitors, but the present work is the first application of these techniques to methylphenidate analogs.

2. Results

The structures of the 80 molecules of the (\pm)-*threo*-MP analog data set are listed in Table 1 along with their DAT binding affinities. Binding affinity is expressed as an IC₅₀ (that concentration of compound required to inhibit the specific binding of [³H]WIN 35,428 in control samples by 50%). All the molecules share an important feature: a common scaffold consisting of 14 atoms (N₁–C₆, C₁–C₆, C₇, with the 14th atom, C₈, being the first carbon of the R3 side chain; see structure in Table 1). MP is compound **39** with R1 = H, R2 = H, and R3 = CO₂CH₃. These three sites of substitutions on MP (the phenyl ring (R1), the piperidinyl nitrogen (R2), and the side chain (R3)) produce the other 79 analogs in the table.

2.1. Atom-level E-state indices

The atom-level electrotopological state (E-state) indices^{43–52} are a measure of the atom's electron accessibility and topological accessibility in a molecule. They are identified by the numbering scheme on the structure in Table 1. For example, ESN₁ is the atom-level E-state index of N₁, ESC₂ is that of C₂, ESC₁ is that of C₁, etc. For both the nMP and pMP data sets, the atom-level E-state indices of eight scaffold atoms (ESC₂, ESC₃, ESC₄, ESC₅, ESC₆, ESC₇, ESC₁, ESC₆) were found by correlation analysis to be redundant. Table 2 identifies which indices were selected for the training and test set studies, and lists the values of the E-state indices of the 14-atom scaffold of nMP and pMP. Except for ESN₁, the values of the E-state indices are very similar for nMP and pMP. The difference in ESN₁ values is due to the difference in chemical environment of neutral and protonated N₁.

2.2. Identification of test and training sets

The sphere exclusion procedure^{53,54} (see Section 4.1.1.4) resulted in the same test set for both the nMP and pMP data sets, consisting of analogs **11**, **26**, **27**, **30**, **32**, **33**, **34**, **41**, **56**, **57**, **62**, **67**, **71**, and **80**. It is interesting to note how the test set analogs are distributed with respect to changes in R1, R2, and R3, compared to the full data set of 80 analogs. The analogs can be grouped based on all possible combinations of substitutions with respect to the parent compound, MP (compound **39** in Table 1 with R1 = H, R2 = H, and R3 = CO₂CH₃). Table 1 also lists this information for each analog in the column titled 'Groups'. It is also possible to consider the data set such that the substitutions occur *at least* at R1 (this would group analogs for R1, R1 + R2, R1 + R3, and R1 + R2 + R3), *at least* at R2 (R2, R1 + R2, R2 + R3, and R1 + R2 + R3), and *at least* at R3 (R3, R1 + R3, R2 + R3, and R1 + R2 + R3). These additional groupings are shown in Table 3 under R1*, R2*, and R3*, respectively.

Table 3 shows how the full data set (minus MP) is distributed with respect to changes at R1, R2, and R3. The table shows that

the 14 analogs in the test set represent all possible combinations of substitutions. Table 1 shows that the substitution patterns on these 14 test set analogs (18% of the data set) are wide-ranging and representative, as are their binding affinity values which range from 5.3 to 8.8 log units—a difference of greater than three log units. The training set corresponding to this test set contains the complementary 66 analogs (80 – 14), including MP.

2.3. 2D-QSAR study results

Tables 4–6 give detailed results for the nMP 2D-QSAR model.

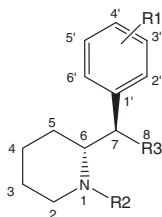
2.3.1. Descriptors

Table 4 lists the 12 most chemically-relevant, nonredundant Molconn-Z descriptors along with the six nonredundant atom-level E-state indices of the scaffold atoms identified earlier. The molecular shape and electrotopological descriptors are discussed in detail in the Molconn-Z manual⁵⁵ and elsewhere.^{44,45,56–58} Briefly, they encode the structure of a molecule by reducing the molecular formula to a hydrogen-suppressed skeleton or 'graph'. Molecular shape indices, such as diam, muldiam, rad, and ishape, characterize the molecular graph. Diam is the graph diameter, muldiam is the multiplicity of the diameter, rad is the graph radius, and ishape is (diam – rad)/rad. Descriptors beginning with 'S' are sums of atom-level E-state indices for all atoms of a particular type in a given molecule. For example, SsF, SsCl, and SsI in Table 4 refer to the sum of the atom-level E-state indices for the F, Cl, and I atom types, respectively. SssO and SssS refer to similar sums for atom types –O– and –S–. SsNH₂, SaaN, and SddsN refer to corresponding sums for N in –NH₂, N with lone pairs in an aromatic ring, and a planar nitrogen with three bonds such as in NO₂, respectively. SHdsCH refers to the sum of the atom-level E-state indices for all hydrogens bonded to a double-bonded carbon (e.g., the H of =CHR).

These 18 descriptors were used as input to the partial least squares (PLS) analysis of the pIC₅₀ of the 66 nMP training set analogs, where pIC₅₀ = –log IC₅₀ with IC₅₀ given in molar units. The table also lists the normalized coefficient and fractional contribution of each descriptor to the PLS model. The table shows that, of the atom-level E-state indices, ESC₂ makes the largest contribution (22%) of all the descriptors, with ESC₃ and ESC₄ contributing about 11% each, and ESC₅ only 3%. Taken together, the E-state indices of the 2', 3', 4', and 5' positions of the phenyl ring contribute 46% to the model. Their large contribution is perhaps not surprising given that 32 out of the 66 training set analogs have substituents on the phenyl ring (i.e., Group R1 of Table 1). In contrast, ESN₁, where N₁ is the point of R2 substitution, and ESC₈, where C₈ is the first carbon of R3 substituent, together contribute only an additional 4% to the model. This indicates that the activity of the analogs is particularly sensitive to substitution on the phenyl ring. This is supported by the fact that the descriptor SsCl contributes an additional 15% to the model. Of the 66 training set analogs, nine have chlorine substituents on the phenyl ring (as the R1 substituents) and five have substituents containing chlorine at the R2 position (see structure of MP at the top of Table 1 for the location of R1 and R2.).

Taken together, the atom-level E-state indices contribute about 50% to the model. They can be used to provide a qualitative interpretation of the SAR data in Table 1. The table shows that analogs that have a 2' position substituent on the phenyl ring have very poor binding affinities (e.g., analogs **45**, **55**, and **56**). This can be explained by examining Eq. (2) and the sign of the coefficients in column two of Table 4. In Eq. (2), the δ value is in the denominator. By definition, replacing the hydrogen substituent on the 2' position carbon with a heavy atom increases that carbon's δ value, thereby decreasing its E-state index (ESC₂) relative to that of the 2' position

Table 1
Methylphenidate analog data set^a



	R1 ^b	R2	R3 ^c	IC50 (nM)	pIC ₅₀ ^d	Groups ^e
1	-H		-CO ₂ CH ₃	422 ± 13	6.37	R2
2	-H	-(CH ₂) ₃ Ph	-CH ₂ OH	194 ± 14	6.71	R2 + R3
3	-H	-CH ₂ C≡CH	-CO ₂ CH ₃	821 ± 100	6.09	R2
4	-H	-(CH ₂) ₄ Ph	-CH ₂ OH	623 ± 64	6.21	R2 + R3
5	-H	-(CH ₂) ₂ Ph	-CH ₂ OH	1430 ± 150	5.84	R2 + R3
6	-H	-(CH ₂) ₃ Ph	-CO ₂ CH ₃	267 ± 13	6.57	R2
7	-H		-CO ₂ CH ₃	106 ± 24	6.98	R2
8	-H	-(CH ₂) ₂ Ph	-CO ₂ CH ₃	678 ± 46	6.17	R2
9	-H	-(CH ₂) ₄ Ph	-CO ₂ CH ₃	205 ± 44	6.69	R2
10	-H	-(CH ₂) ₅ Ph	-CO ₂ CH ₃	1570 ± 80	5.80	R2
11	-H	-(CH ₂) ₆ Ph	-CO ₂ CH ₃	656 ± 17	6.18	R2
12	-H		-CO ₂ CH ₃	243 ± 40	6.62	R2
13	-H	-CH ₂ CH=CH ₂	-CO ₂ CH ₃	597 ± 4.0	6.22	R2
14	-H		-CO ₂ CH ₃	31.2 ± 5.7	7.51	R2
15	-H		-CO ₂ CH ₃	113 ± 3.0	6.95	R2
16	-H		-CO ₂ CH ₃	79.1 ± 1.4	7.10	R2
17	-H		-CO ₂ CH ₃	392 ± 15	6.41	R2
18	-H		-CO ₂ CH ₃	369 ± 4.0	6.43	R2
19	-H		-CO ₂ CH ₃	173 ± 15	6.76	R2
20	-H		-CO ₂ CH ₃	128 ± 13	6.89	R2
21	-H		-CO ₂ CH ₃	536 ± 38	6.27	R2
22	-H		-CO ₂ CH ₃	143 ± 25	6.85	R2
23	-H		-CO ₂ CH ₃	224 ± 1.0	6.65	R2
24	-H		-CO ₂ CH ₃	459 ± 67	6.34	R2
25	-H	-CH ₂ CH ₃	-CH ₂ OH	2340 ± 780	5.63	R2 + R3
26	3',5'-diCH ₃	-H	-CO ₂ CH ₃	4690 ± 60	5.33	R1
27	3',5'-diCl	-H	-CO ₂ CH ₃	65.6 ± 5.4	7.18	R1
28	-H		-CH ₂ OH	25.8 ± 0.20	7.59	R2 + R3

(continued on next page)

Table 1 (continued)

	R1 ^b	R2	R3 ^c	IC ₅₀ (nM)	pIC ₅₀ ^d	Groups ^e
29 ^f	-H	-CH ₂ Ph	-CO ₂ CH ₃	52.9 ± 2.3	7.28	R2
30	-H	-H	-CH ₂ OH	448 ± 8.0	6.35	R3
31 ^g	4'-OH	-H	-CO ₂ CH ₃	98.0 ± 10	7.01	R1
32	3'-CH ₂ OH, 4'-OCH ₂ OH	-CH ₃	-CO ₂ CH ₃	620 ± 40	6.21	R1 + R2
33	4'-OH	-CH ₃	-CO ₂ CH ₃	1220 ± 140	5.92	R1 + R2
34 ^g	4'-NO ₂	-H	-CO ₂ CH ₃	494 ± 33	6.31	R1
35 ^g	3'-NH ₂	-H	-CO ₂ CH ₃	265 ± 5.0	6.58	R1
36 ^g	4'-NH ₂	-H	-CO ₂ CH ₃	34.5 ± 4.0	7.46	R1
37 ^g	4'-OCH ₃	-H	-CO ₂ CH ₃	83.0 ± 11	7.07	R1
38 ^g	4'-Cl	-H	-CO ₂ CH ₃	20.6 ± 3.4	7.69	R1
39 ^g	-H	-H	-CO ₂ CH ₃	83.0 ± 7.9	7.08	-
40 ^g	4'- <i>t</i> -Butyl	-H	-CO ₂ CH ₃	13,500 ± 450	4.87	R1
41 ^h	3'-Cl	-CH ₃	-CO ₂ CH ₃	160 ± 18	6.79	R1 + R2
42 ^g	4'-I	-H	-CO ₂ CH ₃	14.0 ± 0.0	7.85	R1
43 ^g	3'-Br	-H	-CO ₂ CH ₃	4.18 ± 0.17	8.38	R1
44 ^f	4'-CH ₃	-CH ₃	-CO ₂ CH ₃	140 ± 9.0	6.85	R1 + R2
45 ^g	2'-Br	-H	-CO ₂ CH ₃	1870 ± 135	5.73	R1
46 ^g	2'-OCH ₃	-H	-CO ₂ CH ₃	101,000 ± 10,000	4.00	R1
47 ^g	3'-OCH ₃	-H	-CO ₂ CH ₃	288 ± 52	6.54	R1
48 ^g	2'-OH	-H	-CO ₂ CH ₃	23,100 ± 50	4.64	R1
49 ^g	3'-OH	-H	-CO ₂ CH ₃	321 ± 1.0	6.49	R1
50 ^g	3'-Cl	-H	-CO ₂ CH ₃	5.10 ± 1.6	8.29	R1
51 ^g	4'-F	-H	-CO ₂ CH ₃	35.0 ± 3.0	7.46	R1
52 ^g	3',4'-diCl	-H	-CO ₂ CH ₃	5.30 ± 0.70	8.28	R1
53 ^g	3',4'-diOCH ₃	-H	-CO ₂ CH ₃	810 ± 10	6.09	R1
54 ^g	4'-Br	-H	-CO ₂ CH ₃	6.90 ± 0.10	8.16	R1
55 ^g	2'-Cl	-H	-CO ₂ CH ₃	1950 ± 230	5.71	R1
56 ^g	2'-F	-H	-CO ₂ CH ₃	1420 ± 120	5.85	R1
57 ^g	3'-F	-H	-CO ₂ CH ₃	40.5 ± 4.5	7.39	R1
58 ^g	4'-CH ₃	-H	-CO ₂ CH ₃	33.0 ± 1.2	7.48	R1
59 ^g	3'-CH ₃	-H	-CO ₂ CH ₃	21.4 ± 1.1	7.67	R1
60	3'-F	-H	-CH ₂ OH	281 ± 32	6.55	R1 + R3
61	3',4'-diCl	-H	-CH ₂ OH	4.20 ± 0.52	8.38	R1 + R3
62	3',4'-diCl	-H	-CH ₂ OCH ₃	1.70 ± 0.24	8.77	R1 + R3
63	3'-Cl	-CH ₂ Ph	-CO ₂ CH ₃	41.2 ± 3.4	7.39	R1 + R2
64	-H	-CH ₂ Ph	-CON(CH ₃) ₂	1730 ± 52	5.76	R2 + R3
65	-H	-CH ₂ Ph	-CONH ₂	384 ± 8.0	6.42	R2 + R3
66 ^h	-H	-CH ₂ Ph	-CH ₂ OH	23.7 ± 3.3	7.63	R2 + R3
67 ^h	-H	-CH ₂ Ph	-CH ₂ OCH ₃	17.8 ± 1.1	7.75	R2 + R3
68	-H	-H	-CH ₂ OCH ₃	97.1 ± 10.3	7.01	R3
69	3',4'-diCl	-CH ₂ Ph	-CO ₂ CH ₃	76.3 ± 2.7	7.12	R1 + R2
70	3',4'-diCl	-CH ₂ Ph	-CH ₂ OH	2.74 ± 0.35	8.57	R1 + R2 + R3
71	3',4'-diCl	-CH ₂ Ph	-CH ₂ OCH ₃	4.20 ± 1.2	8.38	R1 + R2 + R3
72	3',4'-diCl	-H	-CONH ₂	16.4 ± 2.4	7.79	R1 + R3
73	-H	-H	-CO ₂ CH ₂ Ph	1020 ± 130	5.99	R3
74	3'-CH ₃	-CH ₃	-CO ₂ CH ₃	108 ± 16	6.97	R1 + R2
75	-H	-H	-CH ₂ O(CO)CH ₃	690 ± 270	6.16	R3
76	-H	-H	-CONH ₂	1730 ± 170	5.76	R3
77 ^h	-H	-CH ₃	-CO ₂ CH ₃	499 ± 25	6.30	R2
78	4'-C ₂ H ₅	-H	-CO ₂ CH ₃	737 ± 78	6.13	R1
79 ⁱ	3',4'-Benzo ^j	-H	-CO ₂ CH ₃	11.0 ± 2.5	7.96	R1
80 ⁱ	4'-CF ₃	-H	-CO ₂ CH ₃	615 ± 15	6.21	R1

^a Binding data were generated in the laboratory of MMS; values are expressed as the mean ± standard error of the mean (SEM) of 2–7 assays for each compound. Methylphenidate is compound 39. Compounds **42**, **43**, **45**, and **54** were provided by Dr. S. J. Gately of Brookhaven National Laboratories.

^b Naming convention for R1 substituents is based on the six positions of the phenyl ring; for example, **48** (2'-OH MP) has the -OH substituent at the 2' position of the phenyl ring. For R2 substituents, Ph = phenyl.

^c The first carbon in the R3 substituent is the 14th atom of the scaffold, C₈.

^d pIC₅₀ = -log IC₅₀, with IC₅₀ in molar units.

^e 'Group' refers to the substituents R1, R2, and/or R3, that have been modified compared to MP (**39**).

^f Synthesis and binding studies have been described elsewhere.¹⁶

^g Synthesis and binding studies have been described elsewhere.¹²

^h Synthesis and binding studies have been described elsewhere.¹⁹

ⁱ Synthesis and binding studies have been described elsewhere.¹⁷

^j 'Benzo' refers to a 1,2-disubstituted benzene ring (3',4'-benzo = beta naphthyl analog).

carbon atom in MP. In the regression equation, ESC_{2'} is multiplied by the coefficient 1.017, so if it is assumed that the only change in the 2' position analog relative to MP is in the value of ESC_{2'}, then (IC₅₀ of a MP analog with a 2' position substituent) > (IC₅₀ of MP). In contrast, many analogs with 3' position phenyl ring substituents have better binding affinity than MP (e.g., **57** and **63**). As above, the δ value of a 3' position carbon with a heavy atom substituent is

greater than (and its E-state index (ESC_{3'}) is less than) that of the same carbon in MP. However, in the regression equation ESC_{3'} is multiplied by a negative coefficient, -0.313. This results in the prediction that (IC₅₀ of a MP analog with a 3' position substituent) < (IC₅₀ of MP), in agreement with much of the experimental data in Table 1. A similar analysis pertains to ESC_{4'} and ESC_{5'}. These E-state indices are also multiplied by negative coefficients in the

Table 2
Atom-level E-state indices of scaffold atoms for neutral and protonated methylphenidate

E-State index	nMP	pMP	Redundant ^a
ESN ₁	3.429	4.589	
ESC ₂	0.960	0.835	X
ESC ₃	1.169	1.114	X
ESC ₄	1.148	1.117	X
ESC ₅	0.997	0.941	X
ESC ₆	0.147	0.022	X
ESC ₇	-0.264	-0.319	X
ESC ₈	-0.187	-0.219	
ESC _{1'}	0.950	0.918	X
ESC _{2'}	1.915	1.895	
ESC _{3'}	0.766	0.752	
ESC _{4'}	1.881	1.871	
ESC _{5'}	1.910	1.896	
ESC _{6'}	1.959	1.939	X

^a 'X' indicates a redundant descriptor that was deleted from the final set.

regression equation. The model suggests that substitutions at these positions will lead to lower IC₅₀'s relative to MP. As Table 1 shows, many of the analogs with the best binding affinities (such as analogs 43, 50, 52, and 54) are those that are substituted at these positions. There are some exceptions to this analysis, indicating that it is too simplistic to completely describe the data set. This supports the use of the more detailed CoMFA study described below.

2.3.2. Model validation

In Table 5, the non cross-validated models were produced for the optimal number of components obtained by the cross-validated models. The probability values, or *p*-values, for all non-cross-validated runs are not shown because they were always very small (0.000 to three decimal places). Thus, the probability that *r*² equals zero is itself zero (or very small), signifying the existence of a relationship between the descriptors used in a model and the binding affinity. A stable or robust model is one with high *Q*², low *cSDEP*, and a slope, dq^2/dr_{yy}^2 , near 1.0. Such a model will be affected in proportion to the magnitude of the change in the underlying pIC₅₀ activity values. The *Q*² and *cSDEP* statistics tend to be inversely related. The *Q*² value is a conservative statistic and will usually be low because it is based on randomized or noisy activity values.

Table 5 shows that the 2D-QSAR model (*q*² = 0.358) explains only 55% of the variance in the training set data. The predicted pIC₅₀'s and associated residuals (actual value – predicted value) are given in the Supplementary data. For 23% of the training set, the absolute value of the residual was greater than 0.5; for 9% of the data set, it was between 1.0 and the maximum value, 1.8. However, it should be noted that prior to obtaining this model, 17 descriptors were eliminated from the original set of 29 nonredundant descriptors obtained after correlation analysis. This would reduce the explanatory power of the 2D-QSAR model in Table 5 as

Table 4
Final set of 2D-QSAR descriptors for the nMP data set

Descriptor	Coefficient in regression equation ^a	Normalized coefficient ^b	Fractional contribution to model
Diam	-0.000	0.001	0.000
Muldiam	-0.139	0.083	0.044
lshape	-0.317	0.177	0.094
SHdsCH	0.007	0.008	0.004
SsNH2	-0.031	0.052	0.028
SaaN	0.004	0.004	0.002
SddsN	-0.787	0.042	0.022
SssO	-0.029	0.097	0.051
SsF	-0.016	0.039	0.021
SssS	0.079	0.031	0.017
SsCl	0.068	0.276	0.147
SsI	0.403	0.125	0.066
ESN ₁	0.039	0.022	0.012
ESC _{2'}	1.017	0.407	0.217
ESC _{3'}	-0.313	0.212	0.113
ESC _{4'}	-0.309	0.201	0.107
ESC _{5'}	-0.370	0.053	0.028
ESC ₈	0.220	0.047	0.025

^a Intercept = 6.968.

^b Normalized coefficient is the scaled actual coefficient such that the relative contributions of descriptors become apparent.

the model would not be able to use the orthogonality of the eliminated descriptors to explain the associated variance. Indeed, when the 29 original descriptors were combined with the set of six non-redundant E-state indices, the resulting model explained as much as 74% of the variance. However, this model was considered unsatisfactory because it lacked interpretability due to the presence of a large number of descriptors. This was the reason for conducting variable selection by retaining only the 12 chemically-relevant Molconn-Z descriptors described above.

Table 5 also lists the results of progressive scrambling⁵⁹ for the 2D nMP model. The high value of dq^2/dr_{yy}^2 near 1.0 suggests that this is a stable model, that is, a change in the underlying activity values would produce a proportional change in this model. Validation of the 2D-QSAR model using the test set activity prediction is shown in Table 6. Three (27, 41, and 57) out of the five best-modeled compounds (with residuals less than 0.5) are esters with a halogen substituent at the 3' position of the phenyl ring. The largest residual is for analog 26, which is predicted poorly by the CoMFA models as well (see below). The root mean square deviation (RMSD) of the residuals is 0.98.

2.4. 3D-QSAR studies

The results for the Comparative Molecular Field Analysis (CoMFA)⁶⁰ PLS models for the nMP and pMP data sets are given in Table 5. Both models explain 92% of the variance in the training set data and both have *q*² greater than 0.5. The predicted pIC₅₀'s and residuals for the training set analogs for both models are given in the Supplementary data. For the nMP model, only 6% of the

Table 3
Distribution of data set and test set analogs by substituent groups^a

	R1	R2	R3	R1 + R2	R1 + R3	R2 + R3	R1 + R2 + R3	Total	R1*	R2*	R3*
Data set ^b	29	23	5	7	4	9	2	79	42	41	20
Test set ^c	6	1	1	3	1	1	1	14	11	6	4

^a Analogs that belong to the groups R1, R2, and R3 have a substitution (relative to MP, 39) only at these locations; analogs belonging to the groups (R1 + R2), (R1 + R3), and (R2 + R3) have substitutions at both locations; analogs belonging to the group (R1 + R2 + R3) have substitutions at all three locations. Analogs belonging to groups R1*, R2*, and R3* have at least one substitution at R1, R2, and R3, respectively. See Table 1 for identification of groups R1, R2, and R3.

^b The data set consists of the 79 analogs other than MP in Table 1.

^c The test set consists of analogs 11, 26, 27, 30, 32, 33, 34, 41, 56, 57, 62, 67, 71, and 80.

Table 5
2D- and 3D-QSAR studies: results^a and model validation

Model	Data set	q^2 ^b	SDEP ^c	Compd ^d	r^2 ^e	SEE ^f	F-Value ^g	Q^2 ^h	cSDEP ⁱ	dq^2/dr_{yy}^2 ^j
2D	nMP	0.358	0.734	2	0.550	0.614	38.548	0.251	0.791	0.845
3D	nMP	0.556	0.631	6	0.924	0.261	119.396	0.407	0.727	0.617
3D	pMP	0.568	0.622	6	0.918	0.271	109.644	0.537	0.644	0.759

^a See Section 4.1 for a complete description of parameters and associated mathematical formulae.

^b Cross-validated r^2 statistic.

^c Standard error of prediction after leave-one-out cross-validation.

^d Optimal number of components.

^e Coefficient of determination.

^f Standard error of estimate.

^g Tests null hypothesis that none of the descriptors has any effect on the binding affinity.

^h Expected value of q^2 at the user-specified critical point in Progressive Scrambling.

ⁱ Estimated cross-validated standard error at the user-specified critical point.

^j Slope at the critical point, evaluated with respect to the correlation of the original biological activities versus the scrambled activities.

Table 6
Test set activity^a predictions

Analog	Actual	2D-QSAR (nMP)		3D-QSAR (nMP)		3D-QSAR (pMP)	
		Predicted	Residual ^b	Predicted	Residual ^b	Predicted	Residual ^b
11	6.18	6.65	-0.47	6.50	-0.32	5.95	0.23
26	5.33	7.24	-1.91	7.45	-2.13	7.02	-1.69
27	7.18	7.48	-0.30	8.21	-1.02	7.89	-0.71
30	6.35	6.78	-0.43	6.59	-0.24	6.62	-0.28
32	6.21	7.36	-1.15	4.01	2.20	6.58	-0.38
33	5.92	7.17	-1.26	6.69	-0.78	6.72	-0.80
34	6.31	7.21	-0.91	7.83	-1.52	8.36	-2.05
41	6.79	6.95	-0.15	7.16	-0.36	6.66	0.14
56	5.85	4.58	1.27	6.21	-0.36	6.18	-0.33
57	7.39	7.04	0.35	7.08	0.31	6.73	0.66
62	8.77	7.69	1.08	8.54	0.23	8.69	0.08
67	7.75	6.92	0.83	7.71	0.04	7.25	0.50
71	8.38	7.68	0.70	9.17	-0.79	8.32	0.06
80	6.21	7.42	-1.21	7.71	-1.50	7.27	-1.05

^a Activities are expressed as $pIC_{50} = -\log IC_{50}$ with IC_{50} in molar units.

^b Residual = actual value – predicted value.

training set had a residual with absolute value between 0.5 and the maximum value, 0.6. For the pMP model, only 4% of the training set had a residual with absolute value between 0.5 and the maximum value, 0.85. These results are in contrast to the 2D-QSAR nMP model for which 23% of the training set had an absolute value of the residual greater than 0.5. Both 3D-QSAR models have a high *F*-value, implying that there is a good chance that a relationship exists between the CoMFA predictors (steric and electrostatic field values) and bioactivity measured as pIC_{50} . The (percent steric)/(percent electrostatic) contribution to each model is 46/54 for nMP and 81/19 for pMP. This is a somewhat counterintuitive result as it can be imagined that the electrostatic contribution would be greater for the protonated model than for the neutral model.

2.4.1. Model validation

The results of progressive scrambling are listed in Table 5 for the nMP and pMP 3D-QSAR models. The nMP CoMFA model is stable because its Q^2 is large (0.407) and its slope is fairly good ($dq^2/dr_{yy}^2 = 0.617$). The pMP CoMFA model has a higher Q^2 value (0.537) and a slope nearer to 1.0 ($dq^2/dr_{yy}^2 = 0.759$). The predicted activities of the test set analogs are listed in Table 6. For the nMP model, all but two analogs (**26** and **32**) were predicted with residuals less than 2 units. For the pMP model, just one analog (**34**) had a residual greater than 2 units. The qualitative trends in the test set residuals are generally similar to those of the 2D nMP model. The RMSD of the residuals is 1.09 and 0.86 for the nMP and pMP models, respectively, indicating that the 3D pMP model predicts more accurately than both the 2D and 3D nMP models.

2.4.2. Prediction using models

The nMP and pMP CoMFA models are used to predict the IC_{50} of a MP analog, methyl 2-(naphthalen-1-yl)-2-(piperidin-2-yl)acetate, not in the original data set. The residuals are predicted to be -0.20 and 0.33 by the nMP and pMP models, respectively. This corresponds to predicted IC_{50} values of 448 nM (nMP model) and 1515 nM (pMP model), which are in good agreement with the experimental value of 716 ± 55 nM.¹⁷ Since the residuals are small, both models appear to be useful in predicting the IC_{50} value of a compound closely related to those in the training set.

2.4.3. Interpretation of R1 (phenyl ring substitution) SAR using CoMFA maps

Since most of the SAR changes that lead to significant alterations in binding affinity involve substitution on the phenyl ring, this section will focus on the R1 region. Discussion of the SAR of the R2 and R3 regions is given in Section 3.3. Figure 1 shows the steric and electrostatic CoMFA contour maps for the nMP CoMFA model. The pMP maps are very similar and are not shown. In Figure 1, two orientations were chosen to display the CoMFA contours of the R1 region to best advantage: a 'full view', with the phenyl ring in the plane of the paper and a 'side view', with the molecule rotated 90° so that the phenyl ring is viewed from the side. The maps are essentially a color-coded, three-dimensional summary of the structure-activity relationships of the 66 training set analogs in Table 1. The structures displayed in the maps are those of the test set analogs (Table 6). In the steric maps, the green contours indicate regions where the addition of bulky groups leads to better

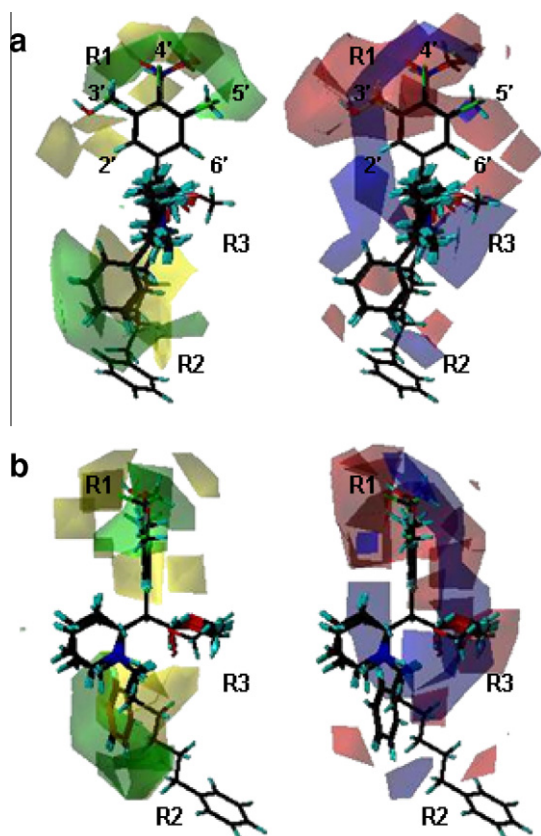


Figure 1. CoMFA maps for nMP (steric on left, electrostatic on right) based on the training set of 66 analogs. Substituent regions (defined in the schematic figure accompanying Table 1) are indicated: R1 (on phenyl ring), R2 (on nitrogen), and R3 (side chain). The 2', 3', 4', 5', and 6' positions on the phenyl ring are noted. The superimposed test set analogs are displayed. Contribution levels: green/yellow = 70/40 and blue/red = 65/25. (a) Full view with phenyl ring in plane of paper. (b) Side view with phenyl ring perpendicular to plane of paper.

binding affinity, whereas the yellow contours indicate regions where steric bulk is not well tolerated. In the electrostatic maps, the blue contours indicate regions where positively charged groups enhance binding affinity, whereas the red contours are regions where negatively-charged groups improve binding affinity. In other words, electron-withdrawing groups are favored as substituents in the red, but not the blue, regions.

Considering analogs with changes in R1 only (see Table 1), it is clear that those analogs that have an electron-withdrawing halogen substituent in the 3' and/or 4' position of the phenyl ring (i.e., analogs **38**, **42**, **43**, **50**, **51**, **52**, **54**, and **57**) have better binding affinity than MP, as does **27**, which has a chlorine atom at both the 3' and 5' positions. Fusion of an aromatic ring onto the 3' and 4' positions, as in the 3',4'-benzo analog, **79**, also gives improved affinity. The 4' position tolerates the addition of $-\text{OH}$ (**31**), $-\text{NH}_2$ (**36**), $-\text{OCH}_3$ (**37**), and $-\text{CH}_3$ (**58**) substituents, but not groups as large as $-\text{C}_2\text{H}_5$ (**78**) or *t*-butyl (**40**). In contrast to their effect at the 4' position, the substituents $-\text{OH}$ (**49**), $-\text{NH}_2$ (**35**) and $-\text{OCH}_3$ (**47**) at the 3' position result in poorer binding affinity compared to MP. This is seen also in the 3',4'-di OCH_3 analog (**53**). However, a $-\text{CH}_3$ substituent at the 3' position (**59**) gives improved binding affinity. All substitutions at the 2' position result in poor binding affinity (see **45**, **46**, **48**, **55**, and **56**).

These trends are summarized in the CoMFA maps. The steric map on the left of Figure 1a shows the presence of favorable green regions off positions 3', 4', and 5' of the phenyl ring, as well as between these positions. The electrostatic map on the right of Figure 1a shows the presence of red regions off positions 3', 4',

and 5' of the phenyl ring. Analogs **27**, **38**, **42**, **43**, **50**, **51**, **52**, **54**, **57**, and **79** all exhibit the appropriate steric bulk and electron density in these regions. Analog **79** has electron density in that region due to the aromatic ring fused between positions 3' and 4' of the phenyl ring, while the other analogs have halogen substituents. The fact that **27**, **38**, **42**, **43**, **50**, **51**, **52**, **54**, **57**, and **79** exhibit the combination of steric and electrostatic requirements shown in Figure 1 is consistent with their improved binding affinity compared to MP. In contrast, **26** has the same steric bulk of **27** (at the 3' and 5' positions) but does not match the electrostatic requirement at those positions. Analog **26** has poor binding affinity compared to MP.

Beyond the green region off position 4' in the Figure 1a steric map lies a yellow region, out of the plane of the aromatic ring, which indicates that large bulky groups such as those of **40** and **78** are unfavorable to DAT binding. This out-of-plane orientation is best noted in the side view of Figure 1b. Similarly, the broad yellow region off the 2' position (Fig. 1a) indicates that substitution in this region is not favorable to binding, as seen in **45**, **46**, **48**, **55**, and **56**. The 3' position tolerates some, but not all, substituents as seen by the unfavorable yellow contours (due to bulkier groups like the $-\text{OCH}_3$ substituent of **47**) lying beyond the green contours (due to the $-\text{Cl}$ (**50**) or $-\text{CH}_3$ (**59**) substituents). Since the methoxy groups are free to rotate, they can occupy the unfavorable yellow regions, described above, which are out of the plane of the aromatic ring.

In summary, halogen substituents at R1 on the phenyl ring, particularly 3',4'-diCl, improve the DAT binding affinity of this series of MP analogs. The steric contour maps show the presence of yellow regions (out of the plane of the aromatic ring) where bulky groups are disfavored. The electrostatic maps show that the π -electron cloud above and below the plane of the phenyl ring lies in the red region where higher electron density is correlated with better binding affinity. This indicates that, in the design of new compounds, the optimal substituents may be those that lie in the plane of the phenyl ring and contain electron-withdrawing groups in the general area of the 3' and 4' positions. The 3',4'-benzo analog has an aromatic group that extends into the favorable green region between the 3' and 4' positions. An area that might be fruitful for exploration is that of halogen substituents on the 3',4'-benzo analog.

3. Discussion

3.1. Test set selection

The test set identification was based upon the selection of the most orthogonal E-state indices. The structural information encoded by the E-state indices allowed the identification of a truly representative subset of analogs that span not only the structure space but also the activity space. Since the particular test set identification technique used in this work is deterministic (i.e., for a given set of input parameters, it identifies the same test set for a given series of analogs), it may eliminate the need for generating a whole collection of test and training sets and repeating model development for each different combination. The input parameters for calculating a test set (described in Section 4.1.1), such as the pairwise correlation coefficient cutoff value, r_{max}^2 , used in the unsupervised forward selection (UFS) procedure,⁶¹ as well as the threshold radius, t , and the particular dissimilarity-based compound selection (DBCS) algorithm^{62,63} used, may be varied to suit the modeler's preferences. Two other test sets were selected using the following combinations (r_{max}^2 , t , DBCS algorithm) = (0.99, 0.10, SE-MinMax) and (0.85, 0.15, SE-MinMax), where SE-MinMax⁶³ is a selection criterion for sphere exclusion (SE) in which the compound with the smallest maximum dissimilarity is selected. The

distribution of resulting test set analogs among the various groups in Table 3 was not as representative of the full data set, as was that shown in the table, derived with $(r_{\max}^2, t, \text{DBCS algorithm}) = (0.85, 0.10, \text{SE-MinMax})$.

The in-house program D-SIM version 1.0 (see Section 4.1.1.4) allows the user to vary the value of t and offers a choice of three sphere-exclusion algorithms. The program output includes a log file with a record of the order in which the analogs are selected in the test set. This information can give some idea about the distribution of the analogs as points within the descriptor space. Thus, analogs that are selected in succession would be closer to each other in the descriptor space. Also, analogs that are selected earlier would lie toward the center of the descriptor space. As an example, in this work, the order of selection for the test set was **11, 80, 67, 41, 56, 32, 71, 27, 33, 57, 62, 30, 26, and 34**. It could be imagined that, as it nears completion, the sphere exclusion algorithm would select the analogs located near the extremes of the descriptor space. If the descriptor space is sparse (due to the series of analogs being 'incomplete'), it is likely that the analogs that are included late in the test set might be outliers. Note that analog **34** in the test set was the last to be selected and had the largest residual from the pMP PLS model. Analog **26**, which was selected just before analog **34**, also had consistently large residuals.

3.2. Preliminary models

The work described herein was not intended to be a comprehensive comparison of 2D descriptor versus 3D CoMFA models, nor an attempt to identify an optimal variable selection technique. These studies are available elsewhere.^{54,64–71} Rather the goal of the present work was to use complementary 2D- and 3D-QSAR modeling to identify the most significant molecular features that relate to the DAT binding affinity of a set of 80 MP analogs. The simple, preliminary models produced by these 2D- and 3D-QSAR studies identified phenyl ring modification as a major determinant of DAT binding affinity and suggest that region as a focus area for future modeling studies. However, it should be noted that 42 out of 80 compounds in the data set have phenyl ring substitutions, so that the data set itself contains more information on the SAR of this region than others.

For the 2D-QSAR model, $\text{ESC}_{2'}$ contributes by far the largest amount (22%) to the model, followed by $\text{ESC}_{3'}$ and $\text{ESC}_{4'}$ at 11% apiece and $\text{ESC}_{5'}$ at 3%. This indicates that substitution at the 2', 3', 4', and 5' positions of the phenyl ring can dramatically affect DAT binding affinity, accounting for almost 50% of the model. Except for ESN_1 , the E-state index of the nitrogen, which is either neutral or protonated depending on the model, the E-state indices are very similar for nMP and pMP.

The nMP and pMP CoMFA models both explain 92% of the variance in the training set data and have q^2 greater than 0.5. Both models are stable. The CoMFA maps identify regions that cannot tolerate steric bulk to be those that lie off the 2' position of the phenyl ring, as well as above and below the phenyl ring near the 3', 4', and 5' positions. Suggested alterations to be explored in the design of new compounds are the placement at the 3' and 4' position of the phenyl ring of electron-withdrawing groups that lie chiefly in the plane of the ring, for example, halogen substituents on the 3',4'-benzo analog.

3.3. Additional SAR insights

Considering the 23 analogs with changes in R2 only, it appears that substitution at the piperidinyll nitrogen usually decreases the affinity of the resulting compounds. Twenty of the 23 compounds exhibit losses of potency ranging from 1.3- to 19-fold compared to MP; the three exceptions are **14, 16, and 29** (all contain benzyl (Bn)

substitutions at R2). It is clear from Table 1 that having more than one methylene group in the substituent $-(\text{CH}_2)_x\text{Ph}$ leads to poor binding affinity. Compare **29**, a good binder with $x = 1$, to the poor binders with increasing chain length $x = 2-6$ (i.e., **8, 6, 9, 10, and 11**). The effect of chain length shows up in the steric maps as yellow contours in the R2 region of Figure 1. Similarly, the effect of substitution on the phenyl ring of $-\text{CH}_2\text{Ph}$ is observed by comparing the binding affinity of **29** to that of **12, 7, and 14** with $-\text{Cl}$ in the *ortho*, *meta*, and *para* positions, respectively. Table 1 shows that only substitution at the *para* position is favorable, as indicated by the green contour off that position in Figure 1.

Four pairs of compounds allow comparison of the effect of R2 substitution when the original phenyl ring of MP contains substitutions, but the ester at R3 remains unchanged. In all four cases, when the R1 substituent is held constant, introduction of a substituent at the nitrogen decreases the affinity of the resulting compound by 4.2- to 31-fold (compare **58 vs 44, 31 vs 33, 52 vs 69, and 50 vs 41**).

Only five analogs have changes solely at R3 (**30, 68, 73, 75, 76**). On average, these compounds were 10-fold less active than MP. The order of increasing activity for those compounds with small substituents at R3 [**76** (amide at R3) < **30** (alcohol) < **68** (ether) \approx **39** (ester, MP)] mostly parallels the order of decreasing polarity, indicating that electronic effects are important. This also agrees with literature results for the even more polar carboxylic acid (ritalinic acid, 2-phenyl-2-(piperidin-2-yl)acetic acid) which is reported to have an $\text{IC}_{50} > 10,000$ nM in another test system.¹⁰ However, the poor activity of ester analogs with more bulky groups at R3 (**73** and **75**) indicates that not much steric bulk can be accommodated at the R3 position.

Of the nine analogs with substituents at both R2 and R3, those with $-\text{CH}_2\text{Ph}$ at R2 and $-\text{CH}_2\text{OH}$ (**66**) or $-\text{COCH}_3$ (**67**) at R3 give improved binding affinity, as does **28** with a chlorine at the *meta* position of the R2 phenyl ring and $\text{R3} = \text{CH}_2\text{OH}$. Of the four analogs that have changes both at R1 and R3, those that have 3',4'-diCl at R1 (**61, 62, and 72**) have improved binding affinity compared to MP, whereas **60** (with 3'F at R1) does not. In fact, with the notable exception of **69**, all analogs that have 3',4'-diCl at the R1 position (**52, 61, 62, 70, 71, and 72**) have greatly improved affinity compared to MP, regardless of their R2 and R3 substituents. Similarly, of the seven analogs that have changes at R1 and R2 (**32, 33, 41, 44, 63, 69, and 74**), those with $-\text{Cl}$ substituents at the 3' position of the R1 phenyl ring and $-\text{CH}_2\text{Ph}$ at R2 (**63** and **69**) have equivalent or better binding affinity compared to MP. As in the discussion of R1 substituents, very bulky groups at the 3' or 4' position are not well tolerated as shown by the poor binding affinity of **32**.

3.4. Future work

The results of CoMFA studies are known to be sensitive to the template conformer used for alignment of all the analogs.⁷² Only the global energy minimum (GEM) conformer was used as a template in the present study. Yet, it is known that molecules do not necessarily bind to proteins in their GEM conformations^{73–77} and the importance of considering conformers other than the GEM in pharmacophore modeling has been demonstrated.^{42,78–84} Therefore, the next step in the development of a 3D-QSAR model for the DAT binding of MP analogs will be to include alternative conformers as templates for MP CoMFA studies. Our recent conformational analysis of nMP and pMP²⁶ identified such conformers by comparison of MP conformers to the structure of a rotationally restricted analog⁸ that has the same DAT binding affinity as MP.¹⁸ Therefore the preliminary studies described here pave the way for our more extensive CoMFA studies of MP analogs with only phenyl ring substitutions.

4. Methods

4.1. Computer modeling

SYBYL⁵⁵ molecular spreadsheets were constructed for two types of data sets: neutral analogs (nMP) and analogs protonated on N₁ (pMP). The nMP data set was used for the 2D-QSAR studies; both data sets were used for the CoMFA studies. The 2D-QSAR study involves generation of hundreds of conformation-independent descriptors, followed by variable selection through complete correlation analysis to identify a set of least redundant descriptors. The 3D-QSAR CoMFA study uses steric and electrostatic conformation-dependent descriptors. In these studies, PLS analysis relates the DAT binding affinity of the 80 MP analogs to structural alterations of a common 14-atom scaffold.

4.1.1. Use of atom-level E-state indices in test set selection

The identification of a test set of analogs is an important part of a model validation strategy.^{85,86} However, care must be taken to select the analogs for constructing the test set. The test set analogs should span both the structure space as well as the activity space. Maw and Hall²⁷ demonstrated the utility of using the atom-level E-state descriptors of a common 19-atom tropane scaffold in their 2D-QSAR study of a data set of 25 tropane dopamine reuptake inhibitors. Here we use the atom-level E-state indices of the common 14-atom scaffold of MP analogs in a different manner: to identify a test set that spans descriptor space for use in both 2D- and 3D-QSAR studies of the MP data set (see Table 1), the assumption being that the variations in the binding affinity may be correlated with the variations in structure due to substitutions on the scaffold atoms.

First, variable selection through correlation analysis was used to delete redundant E-state descriptors from the set of 14. Next, the remaining, nonredundant E-state indices were range-scaled and used to construct a dissimilarity matrix, *D*, the elements of which are the complements of pairwise Tanimoto coefficients.⁸⁷ This dissimilarity matrix was then used along with a sphere exclusion algorithm^{53,54} for identifying a deterministic test set using a dissimilarity-based compound selection (DBCS) algorithm.^{62,63} This ensures that this procedure will always identify the same test set given the same input parameters. The training set was defined as the remaining analogs. The same test and training sets were used for the 2D- and 3D-QSAR studies. The steps are described in detail below.

4.1.1.1. Calculation of E-state indices of scaffold atoms. The atom-level E-state index of atom *i*, *S_i*, is a combination of electronic and topological information defined by⁴⁵

$$S_i = I_i + \sum_j \Delta I_{ij} \quad (1)$$

where *j* indicates all atoms other than *i*. The atom intrinsic state, *I_i*, is defined as

$$I_i = \frac{(2/N_i)^2 \delta_i^v + 1}{\delta_i} \quad (2)$$

where the simple delta value, δ , is the number of electrons of atom *i* in sigma orbitals minus the number of hydrogen atoms bonded to atom *i*; the valence delta value, δ_i^v , is the simple delta value plus the number of electrons of atom *i* in π orbitals plus the number of electrons of atom *i* in lone pair electron orbitals; and *N_i* is the principal quantum number of atom *i*. The perturbation due to all the other atoms in the molecule, ΔI_{ij} , is given by

$$\Delta I_{ij} = (I_i - I_j)/r_{ij}^2 \quad (3)$$

where *r_{ij}* is the graph distance between *i* and *j*. The atom-type E-state index is the sum of the atom-level E-state indices for all the

atoms of a particular atom type.⁵⁸ The E-state index for an atom in a molecule is a measure of both the electron accessibility and the topological accessibility of that atom.

The atom-level E-state indices for the 14 scaffold atoms were calculated by the Molconn-Z module in SYBYL. The scaffold atoms were numbered identically in all analogs. For each molecule, Molconn-Z was used to generate a '.S' file containing the atom-level E-state indices of all atoms in the molecule. The E-state indices for the 14 scaffold atoms were extracted from each .S file and used for all subsequent calculations.

4.1.1.2. Variable selection: identification of redundant E-state descriptors.

Complete correlation analysis was performed on the unscaled atom-level E-state indices of the 14 scaffold atoms to select an 'ideal' or 'minimal' set of descriptors to be used for the calculation of the dissimilarity matrix. A program developed by Whitley et al.⁶¹ (available from <http://www.vclab.org/lab/ufsf/>), which implements the unsupervised forward selection (UFS) algorithm,⁶¹ was used to select the least redundant (or most orthogonal) descriptors. This algorithm first selects the two descriptors that have the smallest pairwise correlation coefficient. Next, it rejects each of the remaining descriptors whose pairwise correlation coefficient with the first two descriptors exceeds a user-specified value, $r_{\max}^2 < 1$. In the present work, r_{\max}^2 was set equal to 0.85. The algorithm then iterates until all descriptors are either selected or rejected. A descriptor is selected if it has the smallest squared multiple correlation coefficient (of the present set of as-yet-unselected descriptors) with the previously-selected descriptors. All descriptors that have squared multiple correlation coefficients with currently-selected descriptors greater than r_{\max}^2 are rejected. Since the selection of additional descriptors is based upon their correlation with those already chosen, the algorithm builds a subset of descriptors that is as orthogonal as possible. Six atom-level E-state indices were selected by the UFS procedure. These were then range-scaled for input to the calculation of the dissimilarity matrix below. Range scaling was performed as

$$z_i = \frac{x_i - x_{\min}}{x_{\max} - x_{\min}} \quad (4)$$

where *z_i* is the scaled descriptor, *x_i* is the unscaled descriptor, and *x_{min}* and *x_{max}* are the respective minimum and maximum values for this descriptor in the data set.

4.1.1.3. Calculation of the dissimilarity matrix. The Tanimoto coefficient is frequently used in the determination of intermolecular similarities and database searching applications.^{63,86,88–90} The pairwise Tanimoto coefficient, *T*, for the similarity between two molecules, *M_i* and *M_j*, is given by

$$T(M_i, M_j) = \sum_{k=1}^m \frac{E_{ik}E_{jk}}{E_{ik}^2 + E_{jk}^2 - E_{ik}E_{jk}} \quad (5)$$

where *M_i* and *M_j* are the *i*th and *j*th analogs; *i, j* = 1, 2, ..., *n*, with *n* = 80 for the MP data set; *k* = 1, 2, ..., *m*, where *m* is the number of nonredundant, atom-level scaffold atom E-state indices selected by the UFS procedure (*m* = 6 in the present application). The *E*'s in Eq. (5) are the atom-level E-state indices for the molecules being used in the current calculation. Note that for *i* = *j*, *T_{ij}* = 1.

The elements of the dissimilarity matrix, *D*, are then the complement of the Tanimoto coefficients obtained above in the similarity matrix, *T*, and are given by

$$D(M_i, M_j) = 1 - T(M_i, M_j) \quad (6)$$

Thus, for *i* = *j*, dissimilarity *D* = 0. The complement of the Tanimoto coefficient is also known as the Soergel distance.

4.1.1.4. Selection of the test set. A sphere-exclusion⁵³ (SE) dissimilarity-based compound selection (DBCS) algorithm was used to select a structurally-diverse test set that spans the biological activity space.⁹¹ Sphere-exclusion algorithms use a predefined value of a 'threshold dissimilarity', t , and in each iteration reject all compounds in the remaining data set that have a dissimilarity less than t with respect to a compound in the current test set. Thus, t defines the radius of a sphere in the descriptor space and at each stage compounds lying within this sphere are excluded from further consideration as candidates for the test set. The size of the resulting test set is determined by the choice of t : a smaller t would generate a larger test set, and vice versa. The algorithm executes as long as there remain compounds in the data set that lie outside all current spheres. A value of 0.15 has been suggested for t ;^{91,92} $t = 0.10$ was used in the present work. The SE-MinMax⁶³ selection criterion for sphere exclusion, in which the compound with the smallest maximum dissimilarity is selected, was used in the present work. An in-house C++ program (D-SIM Version 1.0) was developed for fast, automated test set identification based on various combinations of t and sphere exclusion selection criteria. Once the analogs in the test set were identified, the remaining compounds formed the training set.

4.1.2. Partial least squares analysis of training set analogs

Partial least squares (PLS) analysis was carried out using SYBYL to model the pIC₅₀ values of the 66 training set analogs in terms of various descriptors. The types of descriptors used in each study are described in detail in the 2D-QSAR Study and 3D-QSAR Study sections below. The nMP data set was used in the former study; CoMFA studies were carried out for both the nMP and pMP data sets. The PLS method has been shown to work effectively for matrices such as those encountered in QSAR studies.^{93–96} The leave-one-out cross-validation method was used to calculate the cross-validated r^2 (or q^2), the standard error of prediction (SDEP), and the optimum number of components. The maximum number of components allowed in a model was six. Non-cross-validated PLS models used the optimum number of components identified in the cross-validated run.

In the leave-one-out cross-validation procedure, one analog (or row) in the data set was deleted and a QSAR equation was derived from the remaining analogs (or rows). The binding affinity of the deleted analog was predicted using the derived equation and the deviation from its experimental value (residual) was calculated. The procedure continued until every analog was deleted once and its residual was calculated. The sum of all the squared residuals was calculated as the PRESS (predictive residual sum of squares) statistic. The PRESS statistic was used to calculate the cross-validated correlation coefficient (q^2) and the cross-validated standard error of prediction (SDEP). The q^2 is given by

$$q^2 = 1 - \left(\frac{\text{PRESS}}{\text{SS}} \right) \quad (7)$$

where SS is the sum of squared deviations from the mean.

4.1.3. Model validation

The QSAR models were validated using both activity shuffling (progressive scrambling) and external test set validation.

4.1.3.1. Progressive scrambling. Progressive scrambling⁵⁹ is recommended for large, redundant data sets that have been used to generate models employing cross-validation techniques such as the leave-one-out cross-validation procedure that was used in this work. Three main statistics are generated: (1) *cSDEP* (which is the estimated cross-validated standard error at a user-specified 'critical point'), (2) Q^2 (which is the expected value of q^2 at the specified critical point), and (3) dq^2/dr_{yy}^2 (which is the slope, at

the critical point, evaluated with respect to the correlation of the original activities vs the scrambled activities). Given a redundant data set, the value of Q^2 is considered conservative such that a fairly low value of Q^2 might indicate a robust original model. A value greater than 1.2 for the slope is considered to indicate an unstable model, that is, a model that changes greatly with small changes in the underlying activity values.⁹⁷

Progressive scrambling was performed in SYBYL with 50 scramblings using a maximum of 10 bins to a minimum of 2 bins. The critical point was specified at the default value of 0.85 and the random seed for every scrambling analysis was set to 123456.

4.1.3.2. Test set validation. External validation of selected models was performed using the test set identified above. The activities of the test set analogs were predicted using these models and the residuals were noted.

4.1.4. 2D-QSAR study

The six atom-level E-state indices of the scaffold atoms identified in the test set section above were combined with selected Molconn-Z descriptors to form an input set of descriptors for PLS analysis. The Molconn-Z descriptors were selected as follows: 524 descriptors (other than specific atom-level E-state indices) were calculated for each of the 80 nMP analogs using the Molconn-Z module of SYBYL. The same type of correlation analysis using the UFS algorithm was applied to these descriptors as to the atom-level E-state indices of the scaffold atoms in the test set selection section above, resulting in 29 nonredundant Molconn-Z descriptors. Of these, the 12 most chemically-relevant descriptors were selected by inspection. The deleted descriptors were related to vertex properties, simple cluster counts, count of bromine atoms, maximum atom-level E-state and maximum hydrogen atom-level E-state indices, sums of internal hydrogen bonding E-state indices, and sums of various carbon atom E-state indices. The final set of 12 nonredundant Molconn-Z descriptors contained descriptors related to molecular shape and diameter, and sums of nitrogen, oxygen, fluorine, chlorine, iodine, and sulfur E-state indices, discussed in detail in Section 2. This set of 12 Molconn-Z descriptors was combined with the six nonredundant atom-level E-state indices of the 14-atom scaffold to form a set of 18 descriptors for PLS analysis of the binding affinity of the 80 MP analogs. The PLS analysis and model validation were carried out as described above.

4.1.5. 3D-QSAR study

Separate CoMFA studies were carried out for the nMP and pMP data sets. The CoMFA steric and electrostatic descriptors were calculated for each data set using cutoffs of 30 kcal/mol each and standard CoMFA scaling.

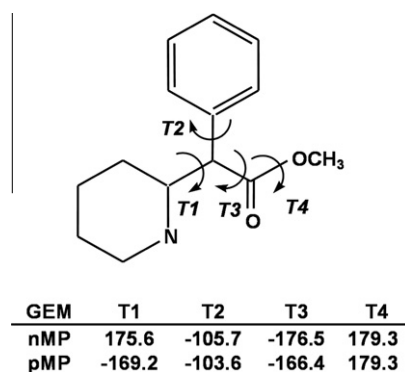


Figure 2. Torsional angles of the neutral (nMP) and protonated (pMP) methylphenidate global energy minimum (GEM) structures. Angles in degrees.

4.1.5.1. Data preparation. The respective nMP and pMP GEM conformations (see Fig. 2) from our previous extensive conformational analysis study of the potential energy surface of MP²⁶ were selected as templates for the CoMFA studies. The active, (+)(*R,R*)-*threo*-methylphenidate stereoisomer [(*R*)-methyl 2-phenyl-2-((*R*)-piperidin-2-yl)acetate]^{12,98} was used to model MP and all the analogs. All 80 analogs were constructed in conformations with torsional angles T1–T4 (see Fig. 2) similar to those of the respective template GEM conformers to give the three-dimensional nMP and pMP data sets. As each analog was built, systematic search followed by energy minimization was carried out to locate the GEM conformer for the analog. In a few cases (described below) the analog's GEM conformer differed significantly from the template's GEM due to significant differences in T1. In those cases, a low-energy structure of the analog with T1 similar to that of the template was selected instead so that all analogs in the series would have the same relative alignment for the CoMFA study.

4.1.5.1.1. Neutral MP data set. For each analog, the piperidine ring was maintained in the chair configuration and its substituents were constructed in the equatorial positions. The energy of the analog was minimized using the MMFF94⁹⁹ force field and charges. Systematic search was performed in 30° increments on all non-ring torsional angles in the analog and the resulting conformations were ranked by energy. As implemented in SYBYL, systematic search increments each specified torsional angle by the specified increment, examines the resulting conformations for van der Waals contacts, and calculates the energy of each conformation without geometry optimization. A 20 kcal/mol cutoff was used during the systematic search to eliminate high energy conformations and to speed up the search. The lowest energy conformation from the systematic search was selected and its geometry was optimized by minimization of its energy. If this new, energy-minimized conformation had a lower energy than that of the analog prior to systematic search, then the new conformation was selected for the data set, otherwise the original was kept. The resulting analogs were aligned on the five central atoms (C₆, C₇, C_{1'}, C₈ and the hydrogen on C₇; see schematic structure of MP in Table 1).

There was one exception to the above procedure. For analog **48** (2'-OH nMP), the above procedure led to hydrogen bonding between the oxygen of the 2' position phenyl substituent and the hydrogen on the piperidinyll nitrogen. This distorted the analog significantly from the template nMP GEM conformation. An alternative conformation was chosen in which the phenyl ring was rotated by 180°, causing the 2'-OH substituent to move out of the way of the piperidine ring while still maintaining the basic nMP GEM conformation.

4.1.5.1.2. Protonated MP data set. The procedure outlined above for the nMP data set (analog construction, minimization, systematic search, and selection) was also followed for the pMP data set. However, the presence of the proton on the nitrogen atom in pMP affects the rotational barrier around T1 compared to nMP.²⁶ This effect was also noted in some pMP analogs (**2, 4, 5, 25, 28, 66, 70, 71, and 75**) that have a somewhat different conformational potential energy surface than pMP. In these cases, the protonated analog's GEM conformer has a very different T1 than that of the pMP GEM conformer. The hydrogen bonding observed between the ester carbonyl oxygen and the hydrogen on the nitrogen of the pMP GEM conformer²⁶ does not occur in these analogs' GEM conformers. So, for these nine analogs, the systematic search was repeated, but torsional angle T1 was frozen at the pMP GEM value. The GEM conformer from this search was selected and the side chain was oriented such that it assumed the same hydrogen bonding orientation as that of the pMP GEM conformation, producing a pMP-like conformer.

4.1.5.2. PLS analysis and model validation. The PLS analysis and model validation were carried out as described above. The col-

umn filtering value for cross-validated CoMFA models was set to 2.0 kcal/mol. Three-dimensional steric and electrostatic CoMFA maps were generated for the CoMFA models and used to interpret the SAR data in Table 1.

4.2. Pharmacology

The binding protocol has been described in detail elsewhere.^{12,19} Briefly, a P₂ fraction was prepared from the striatal tissue of the brains of male Sprague–Dawley rats which had been anesthetized with CO₂ gas. This crude synaptosomal preparation was homogenized in 25 mM sodium phosphate buffer, pH 7.7, at 0 °C using a Tekmar tissueizer. Following a 2 h incubation of the tissue preparation with the analog to be assayed or water (controls) in the presence of 2 nM [³H]WIN 35,428, the samples were rapidly filtered through glass microfiber filters mounted in Millipore filtration manifolds. The bound radioactivity was extracted from the filters using liquid scintillation fluid and counted on a liquid scintillation counter. Amfonelic acid (10 μM final concentration) was used to define nonspecific binding. The K_D for [³H]WIN 35,428 binding was 18.3 ± 0.9 nM.

4.3. Experimental

4.3.1. Chemistry

The syntheses of 47 new compounds (structures shown in Table 1) are presented in this work. All compounds in Table 1 are racemic and are the *threo* isomer. Compounds **26, 27, 72, 76, and 78** were made using our modified phenylacetonitrile method.^{12,19} All of the others were synthesized by straightforward functional group manipulation of known compounds we had previously made, some substituted at R1 and some not. Table 7 outlines the synthetic methods used for each type of compound. Section 4.3.2 gives the details of the synthetic methods.

4.3.1.1. Synthetic modifications on nitrogen (R2) and of the ester group (R3). Compounds **2, 4, 5, and 25** were made by method 1.

4.3.1.2. Synthetic modifications on nitrogen (R2). Compounds **3 and 13** were made by method 2. Compounds **6,–11 and 21–24** were made by method 3. Compounds **7, 63, and 69** were made by method 4. Compounds **12, 14, 15, 16, 17, 18, 19, 20, and 28** were made by method 5. Compounds **32 and 33** were made by method 7. Compound **74** was made by method 13. Compound **1** was made by method 15.

4.3.1.3. Synthetic modifications of the ester group (R3). Compounds **30, 60, 61, and 70** were made by method 6. Compound **62** was made by method 8. Compounds **64 and 65** were made by method 9. Compound **68** was made by method 10. Compound **71** was made by method 11. Compounds **73 and 75** were made by methods 12 and 14.

4.3.2. General methods

Starting materials were purchased from Aldrich Chemical Co. and used without further purification. Tetrahydrofuran (THF) was dried over sodium benzophenone ketyl prior to distillation under Argon. Flash chromatography was run using 230–400 mesh silica gel. Melting points were determined on a Mel-Temp apparatus and are uncorrected. ¹H (300 MHz) spectra were obtained on a Varian Gemini-300 Spectrometer. High-resolution mass spectra [EI (electron ionization), CI (chemical ionization) or FAB (fast atom bombardment)] were recorded on a VG Analytical 70-SE mass spectrometer equipped with a 11–250J data system. Elemental analyses were obtained from Atlantic Microlabs, Atlanta, GA. Free

Table 7
Outline of methods.

Method	Brief outline of reagents
1	Free base in CH ₂ Cl ₂ , add acid chloride, isolate amide, reduce with LiAlH ₄ . See compound 2 ^a
2	Free base in acetone, add alkyl bromide. See compound 13 ^a
3	HCl salt in MeOH, add Et ₃ N and aldehyde then NaBH ₃ CN. See compound 21 ^a
4	Free base in DMF, add K ₂ CO ₃ and benzyl bromide. See compound 7 ^a
5	Free base in acetone, add alkyl chloride and KI. See compound 14 ^a
6	Free base in ether, add LiAlH ₄ . See compound 61 ^a
7	Free base in HCO ₂ H add formaldehyde. See compound 32 ^a
8	Free base in chloroform add (BOC) ₂ O, isolate <i>N</i> -BOC alcohol, treat with KOH/DMSO followed by CH ₃ I, isolate ether, treat with TFA. See compound 62 ^a
9	Ester treated with concentrated HCl, isolate acid, treat with DMF + SOCl ₂ , add appropriate amine. See compound 65 ^a
10	Free base in MeOH, add Pd/H ₂ . See compound 68 ^a
11	Free base in DMSO, treat with KOH/DMSO followed by CH ₃ I. See compound 71 ^a
12	Ester treated with HCl, isolate acid, treat with benzyl alcohol. See compound 73 ^a
13	Free base in MeOH, add formaldehyde and acetic acid, Pd/H ₂ . See compound 74 ^a
14	Alcohol treated with acetyl chloride. See compound 75 ^a
15	Nitro compound in EtOAc, 5% Pt/C, H ₂ , isolate amine, treat with CS ₂ . See compound 1 ^a

^a Details of the method used to synthesize each compound can be found in Section 4.3.2.

bases were dissolved in EtOAc or MeOH and converted to HCl salts by the addition of 1 M HCl (1.5 equiv) in diethylether. The excess HCl was removed under reduced pressure and the solid was recrystallized from various mixtures of MeOH and EtOAc. Nomenclature of compounds: methylphenidate is methyl 2-phenyl-2-(piperidin-2-yl)acetate, ritalinic acid is 2-phenyl-2-(piperidin-2-yl)acetic acid and ritalinol is 2-phenyl-2-(piperidin-2-yl)ethanol. All structures are shown in Table 1.

4.3.2.1. (±)-*threo*-*N*-(4-Isouthiocyanantobenzyl)methylphenidate (1).

A mixture of 400 mg of compound **15**, 90 mg of 5% Pt/C and 15 mL EtOAc was exposed to H₂ at 48 psi for 2 h. Filtration and evaporation of solvents gave a solid amine (360 mg) that was mixed with 25 mL of HCl, 15 mL water, 350 mg NaHCO₃ and 90 μL of CS₂. After 15 min of vigorous stirring, the organic layer was dried and evaporated. The solid was recrystallized from EtOAc to give 292 mg of the pure final product which showed: mp 112–113 °C; ¹H NMR (CDCl₃): δ 1.60–1.10 (m, 6H), 2.58–2.53 (m, 1H), 3.03–2.95 (m, 1H), 3.66–3.49 (m, 1H), 3.69 (s, 3H), 3.76 (d, 1H, *J* = 13.3 Hz), 3.94 (d, 1H, *J* = 13.3 Hz), 4.16 (d, 1H, *J* = 10.2 Hz), 7.40–7.20 (m, 9H) ppm; CIMS *m/z* 381.18, calcd for C₂₂H₂₅N₂O₂S (MH)⁺, 381.16. Anal. (C₂₂H₂₄N₂O₂S) C, H, N.

4.3.2.2. (±)-*threo*-*N*-(3-Phenylpropyl)ritalinol (2).

A solution of (±)-*threo*-methylphenidate (0.03 g, 0.13 mmol) in dry CH₂Cl₂ (15 mL) was mixed with anhydrous MgSO₄ (2 g) and anhydrous Na₂CO₃ (2 g). The suspension was vigorously stirred for 15 min before a solution of 3-phenylpropionylchloride (0.24 moles) in dry CH₂Cl₂ (10 mL) was added dropwise over 5 min at rt. The suspension was stirred for 30 min and filtered. The organic layer was washed successively with 1.2 M HCl (100 mL), 25% brine (100 mL), 5% aqueous NaOH (2 × 100 mL), and 25% brine (100 mL) and dried over anhydrous MgSO₄. The residue obtained after removal of solvents was recrystallized in a minimum amount of hot methanol. In all cases the ¹H NMR (CDCl₃) was complicated due to amide rotomers, but was consistent with the expected product. The amide (1 equiv) was dissolved in anhydrous Et₂O and cooled in an ice-bath for 15 min. A solution of LiAlH₄ in ether (1 M, 5 equiv) was added and the mixture was stirred in an ice-bath for an additional 5 min. The resulting mixture was heated under reflux for 2 h, and then cooled in an ice-bath. Unreacted LiAlH₄ was quenched by careful addition of excess water (80 mL). The ether layer was separated and washed with water (2 × 50 mL), dried (MgSO₄), and evaporated in vacuo to give a residue. The hygroscopic hydrochloride salt was prepared and converted to the free base with 10% Na₂CO₃ solution, extraction with EtOAc

and evaporation of solvents to dryness in vacuo to give a very viscous colorless liquid (75% based on methylphenidate). ¹H NMR (CDCl₃): δ 1.6–0.99 (m, 6H), 1.98–1.81 (m, 2H), 2.75–2.60 (t, 3H), 2.81–2.75 (t, 2H, *N*-CH₂), 3.2–3.1 (d, 1H), 3.38–3.25 (t, 1H), 3.41–3.40 (t, 1H), 3.80–3.75 (dd, 1H, from CH₂OH), 4.0 (t, 1H, from CH₂OH), 7.38–7.10 (m, 10H, aromatic-H) ppm; CIMS *m/z* 324.20, calcd for C₂₂H₃₀NO (MH)⁺, 324.23. Anal. (C₂₂H₂₉NO) C, H, N.

4.3.2.3. (±)-*threo*-*N*-Propargylmethylphenidate-HCl (3).

Using the same method as in the synthesis of **13**, propargylbromide (48 mg, 0.40 mmol) and (±)-*threo*-methylphenidate (89 mg, 0.38 mmol) gave the free amine (100 mg, 81%) was obtained. The hydrochloride salt showed: mp 129–130 °C; ¹H NMR (CDCl₃): δ 1.60–1.10 (m, 6H), 2.28–2.22 (t, 1H), 2.80–2.70 (m, 1H), 3.10–3.00 (m, 1H), 3.45–3.44 (m, 1H), 3.50–3.49 (d, 1H, *J* = 2.5 Hz), 3.61–3.60 (d, 1H, *J* = 2.5 Hz), 3.70 (s, 3H), 4.00–3.90 (d, 1H, *J* = 10.2 Hz), 7.40–7.20 (m, 5H) ppm; CIMS *m/z* 272.160, calcd for C₁₇H₂₂NO₂ (M-Cl)⁺, 272.165. Anal. (C₁₇H₂₂ClNO₂) C, H, N, Cl.

4.3.2.4. (±)-*threo*-*N*-(4-Phenylbutyl)ritalinol (4).

Using the same method as in the synthesis of **2**, 4-phenylbutylchloride gave a very viscous colorless liquid (40 mg, 69% based on methylphenidate). ¹H NMR (CDCl₃): δ 1.6–0.99 (m, 6H), 1.79–1.60 (m, 4H), 2.75–2.60 (t, 3H), 2.81–2.75 (t, 2H, *N*-CH₂), 3.2–3.1 (d, 1H), 3.38–3.25 (t, 1H), 3.41–3.40 (t, 1H), 3.80–3.75 (dd, 1H, from CH₂OH), 4.0 (t, 1H, from CH₂OH), 7.38–7.10 (m, 10H, aromatic-H) ppm; CIMS *m/z* 338.24, calcd for C₂₃H₃₂NO (MH)⁺, 338.24. Anal. (C₂₃H₃₁NO) C, H, N.

4.3.2.5. (±)-*threo*-*N*-(2-Phenylethyl)ritalinol (5).

Using the same method as in the synthesis of **2**, 2-phenylacetylchloride gave a very viscous colorless liquid (45 mg, 71% based on methylphenidate). ¹H NMR (CDCl₃): δ 1.6–0.99 (m, 6H), 2.98–2.80 (t, 3H), 3.15–3.09 (t, 2H, *N*-CH₂), 3.2–3.1 (d, 1H), 3.38–3.25 (t, 1H), 3.41–3.40 (t, 1H), 3.80–3.75 (dd, 1H, from CH₂OH), 4.0 (t, 1H, from CH₂OH), 7.38–7.10 (m, 10H, aromatic-H) ppm; CIMS *m/z* 310.20, calcd for C₂₁H₂₈NO (MH)⁺, 310.22. Anal. (C₂₁H₂₇NO) C, H, N.

4.3.2.6. (±)-*threo*-*N*-(3-Phenylpropyl)methylphenidate-HCl (6).

Using the same method as in the synthesis of **21**, a mixture of methylphenidate hydrochloride (0.16 g) and 3-phenylpropion-aldehyde (0.2 mL) gave the hydrochloride salt (white crystals, 49 mg) which showed: mp 160–161 °C; ¹H NMR (CDCl₃): δ 1.60–0.90 (m, 6H), 1.80–1.60 (t, 2H), 2.40 (m, 1H), 2.80–2.60 (m, 4H), 3.10–3.20 (m, 1H), 3.4 (m, 1H), 3.61 (s, 3H), 4.20–4.10 (d, 1H, *J* = 10.4 Hz), 7.40–7.20 (m, 10H) ppm; CIMS *m/z* 352.22,

calcd for $C_{23}H_{30}NO_2$ ($M-Cl$)⁺, 352.23. Anal. ($C_{23}H_{30}ClNO_2$) C, H, N, Cl.

4.3.2.7. (±)-threo-N-(3-Chlorobenzyl)methylphenidate-HCl (7).

Methylphenidate (267 mg, 1.26 mmol) was dissolved in DMF (10 mL), 1.0 g K_2CO_3 added and the mixture stirred for 20 min. Then 3-chlorobenzylbromide (250 μ L) was added and the resulting mixture was stirred at rt overnight. Ether (50 mL) was added, washed with water (5×15 mL) and dried ($MgSO_4$). After evaporation of the solvent, the off-white solid (300 mg) was purified by silica gel column chromatography (2:98 EtOAc/hexane) to give pure product as a white solid (217 mg, 63%). The HCl salt showed: mp 179–180 °C; 1H NMR ($CDCl_3$): δ 7.42–7.21 (m, 9H), 4.15 (d, 1H, $J = 11.6$ Hz), 3.94 (d, 1H, $J = 13.7$ Hz), 3.79 (d, 1H, $J = 13.2$ Hz), 3.67 (s, 3H), 3.50–3.44 (m, 1H), 2.96–2.91 (m, 1H), 2.58–2.52 (m, 1H), 1.58–1.05 (m, 6H) ppm. CIMS m/z 358.17, calcd for $C_{21}H_{25}ClNO_2$ ($M-Cl$)⁺, 358.16. Anal. ($C_{21}H_{25}ClNO_2$) C, H, N, Cl.

4.3.2.8. (±)-threo-N-(2-Phenylethyl)methylphenidate-HCl (8).

Using the same method as in the synthesis of **21** (with the exception that an aqueous workup procedure was employed in the isolation process), a mixture of methylphenidate hydrochloride (0.16 g) and 2-phenylacetaldehyde (0.2 mL) gave the hydrochloride salt (87 mg, 50%) which showed: mp 154–155 °C; 1H NMR ($CDCl_3$): δ 1.60–0.90 (m, 6H), 2.40 (m, 1H), 2.80–2.60 (t, 2H), 2.95–3.00 (t, 2H), 3.40 (m, 1H), 3.65 (s, 3H), 4.20–4.10 (d, 1H, $J = 10.4$ Hz), 7.40–7.20 (m, 10H) ppm; CIMS m/z 338.22, calcd for $C_{22}H_{28}NO_2$ ($M-Cl$)⁺, 338.21. Anal. ($C_{22}H_{28}ClNO_2$) C, H, N, Cl.

4.3.2.9. (±)-threo-N-(4-Phenylbutyl)methylphenidate-HCl (9).

Using the same method as in the synthesis of **21**, a mixture of methylphenidate hydrochloride (0.172 g), 4-phenylbutyraldehyde (0.19 g, 1.28 mmol) gave the hydrochloride salt (white crystals, 91 mg) which showed: mp 140–141 °C; 1H NMR ($CDCl_3$): δ 1.60–0.90 (m, 6H), 1.80–1.60 (t, 4H), 2.40 (m, 1H), 2.60–2.58 (m, 4H), 3.10–3.20 (m, 1H), 3.4 (m, 1H), 3.61 (s, 3H), 4.20–4.10 (d, 1H, $J = 10.4$ Hz), 7.40–7.20 (m, 10H) ppm; CIMS m/z 366.27, calcd for $C_{24}H_{32}NO_2$ ($M-Cl$)⁺, 366.24. Anal. ($C_{24}H_{32}ClNO_2$) C, H, N, Cl.

4.3.2.10. (±)-threo-N-(5-Phenylpentyl)methylphenidate-HCl (10).

Using the same method as in the synthesis of **21**, a mixture of methylphenidate (0.16 g) and phenylpentylaldehyde (0.2 g, 1.3 mmol) gave the hydrochloride salt (white crystals, 81 mg): mp 136–137 °C; 1H NMR ($CDCl_3$): δ 1.60–0.90 (m, 6H), 1.80–1.70 (t, 4H), 2.40 (m, 1H), 2.50–2.20 (m, 4H), 2.6 (t, 2H), 3.10–3.20 (m, 1H), 3.40 (m, 1H), 3.61 (s, 3H), 4.20–4.10 (d, 1H, $J = 10.4$ Hz), 7.40–7.20 (m, 10H) ppm; CIMS m/z 380.25, calcd for $C_{25}H_{34}NO_2$ ($M-Cl$)⁺, 380.26. Anal. ($C_{25}H_{34}ClNO_2$) C, H, N, Cl.

4.3.2.11. (±)-threo-N-(6-Phenylhexyl)methylphenidate-HCl (11).

Using the same method as in the synthesis of **21**, a mixture of methylphenidate (0.17 g) and phenylhexylaldehyde (0.23 g, 1.3 mmol) gave the hydrochloride salt (white crystals, 81 mg) which showed: mp 136–137 °C; 1H NMR ($CDCl_3$): δ 1.60–0.90 (m, 6H), 1.80–1.70 (t, 4H), 2.40 (m, 1H), 2.50–2.20 (m, 4H), 2.6 (t, 2H), 3.10–3.20 (m, 1H), 3.40 (m, 1H), 3.61 (s, 3H), 4.20–4.10 (d, 1H, $J = 10.4$ Hz), 7.40–7.20 (m, 10H) ppm; CIMS m/z 394.25, calcd for $C_{26}H_{36}NO_2$ ($M-Cl$)⁺, 394.27. Anal. ($C_{26}H_{36}ClNO_2$) C, H, N, Cl.

4.3.2.12. (±)-threo-N-(2-Chlorobenzyl)methylphenidate-HCl (12).

Using the same method as in the synthesis of **14**, a mixture of methylphenidate (89 mg, 0.38 mmol) and 2-chlorobenzylchloride (103 mg, 0.50 mmol) gave 100 mg (78%) titled compound. After chromatography on silica gel, the hydrochloride salt showed: mp 151–152 °C; 1H NMR ($CDCl_3$): δ 1.60–1.10 (m, 6H), 2.58–2.53 (m, 1H), 3.03–2.95 (m, 1H), 3.66–3.49 (m, 1H),

3.69 (s, 3H), 3.76 (d, 1H, $J = 13.3$ Hz), 3.94 (d, 1H, $J = 13.3$ Hz), 4.16 (d, 1H, $J = 10.2$ Hz), 7.40–7.20 (m, 9H) ppm; CIMS m/z 358.158, calcd for $C_{21}H_{25}ClNO_2$ ($M-Cl$)⁺, 358.157. Anal. ($C_{21}H_{25}Cl_2NO_2$) C, H, N, Cl.

4.3.2.13. (±)-threo-N-Allylmethylphenidate-HCl (13).

A mixture of (±)-threo-methylphenidate (89 mg, 0.38 mmol) and allyl bromide (48 mg, 0.40 mmol) in acetone (20 mL) was stirred overnight at rt. The mixture was filtered and the filtrate and the washings were evaporated. The residue was chromatographed on 5 g of silica gel using 5% MeOH in $CHCl_3$ to give 100 mg (80%) pure (by 1H NMR analysis) titled compound. The hydrochloride salt showed: mp 159–160 °C; 1H NMR ($CDCl_3$): δ 1.60–1.10 (m, 6H), 2.70–2.58 (m, 1H), 3.18–3.00 (m, 1H), 3.48–3.39 (m, 1H), 3.40–3.30 (d, 2H), 3.70 (s, 3H), 4.15–4.10 (d, 1H, $J = 10.2$ Hz), 5.20–5.00 (m, 1H), 5.90–5.70 (m, 1H), 7.40–7.20 (m, 5H) ppm; CIMS m/z 274.180, calcd for $C_{17}H_{24}NO_2$ ($M-Cl$)⁺, 274.181. Anal. ($C_{17}H_{24}ClNO_2$) C, H, N, Cl.

4.3.2.14. (±)-threo-N-(4-Chlorobenzyl)methylphenidate-HCl (14).

Using a method similar to that in making **13** (except that 0.25 g KI was added to the reaction mixture, the reaction time was increased to 48 h and the crude product was filtered through a silica gel column), methylphenidate (89 mg, 0.38 mmol) and 4-chlorobenzylchloride (84 mg, 0.40 mmol) gave 70 mg (71%) titled compound. The hydrochloride salt showed: mp 169–170 °C; 1H NMR ($CDCl_3$): δ 7.42–7.21 (m, 9H), 4.15 (d, 1H, $J = 11.6$ Hz), 3.94 (d, 1H, $J = 13.7$ Hz), 3.79 (d, 1H, $J = 13.2$ Hz), 3.67 (s, 3H), 3.50–3.44 (m, 1H), 2.96–2.91 (m, 1H), 2.58–2.52 (m, 1H), 1.58–1.05 (m, 6H) ppm. CIMS m/z 357.17, calcd for $C_{21}H_{25}ClNO_2$ ($M-Cl$)⁺, 357.15. Anal. ($C_{21}H_{25}Cl_2NO_2$) C, H, N, Cl.

4.3.2.15. (±)-threo-N-(4-Nitrobenzyl)methylphenidate-HCl (15).

Using the same method as in the synthesis of **14**, a mixture of methylphenidate (89 mg, 0.38 mmol) and 4-nitrobenzylchloride (86 mg, 0.40 mmol) gave 70 mg (65%) titled compound. The hydrochloride salt was recrystallized from EtOAc/hexane and showed: mp 170–172 °C; 1H NMR ($CDCl_3$): δ 1.60–1.10 (m, 6H), 2.58–2.53 (m, 1H), 3.03–2.95 (m, 1H), 3.66–3.49 (m, 1H), 3.69 (s, 3H), 3.78–3.74 (d, 1H, $J = 13.3$ Hz), 3.96–3.91 (d, 1H, $J = 13.3$ Hz), 4.18–4.14 (d, 1H, $J = 10.2$ Hz), 7.40–7.20 (m, 5H), 8.15 (d, 2H), 8.75 (d, 2H) ppm; CIMS m/z 369.180, calcd for $C_{21}H_{25}N_2O_4$ ($M-Cl$)⁺, 369.189. Anal. ($C_{21}H_{25}ClN_2O_4$) C, H, N, Cl.

4.3.2.16. (±)-threo-N-(4-Methoxybenzyl)methylphenidate-HCl (16).

Using the same method as in the synthesis of **14**, a mixture of methylphenidate (89 mg, 0.38 mmol) and 4-methoxybenzylchloride (63 mg, 0.40 mmol) gave 80 mg (61%) titled compound. The hydrochloride salt was recrystallized from EtOAc/hexane and showed: mp 164–165 °C; 1H NMR ($CDCl_3$): δ 1.60–1.10 (m, 6H), 2.58–2.53 (m, 1H), 3.03–2.95 (m, 1H), 3.66–3.49 (m, 1H), 3.70 (s, 3H), 3.78–3.74 (d, 1H, $J = 13.3$ Hz), 3.85 (s, 3H), 3.96–3.91 (d, 1H, $J = 13.3$ Hz), 4.18–4.14 (d, 1H, $J = 10.2$ Hz), 6.88 (d, 2H, $J = 8.8$ Hz), 7.40–7.20 (m, 7H) ppm; CIMS m/z 354.20, calcd for $C_{22}H_{28}NO_3$ ($M-Cl$)⁺, 354.21. Anal. ($C_{22}H_{28}ClNO_3$) C, H, N, Cl.

4.3.2.17. (±)-threo-N-((5-Chlorothiophene-2-yl)methyl)methylphenidate-HCl (17).

Using the same method as in the synthesis of **14**, a mixture of (±)-threo-methylphenidate hydrochloride (0.040 g, 0.038 mmol) and 2-chloro-5-(chloromethyl)thiophene (0.05 mL, excess) gave the titled compound. The hydrochloride salt was recrystallized from EtOAc/hexane and showed: mp 174–176 °C; 1H NMR ($CDCl_3$): δ 1.6–1.1 (m, 6H), 2.58–2.53 (m, 1H), 3.03–2.95 (m, 1H), 3.66–3.49 (m, 1H), 3.71 (s, 3H, OCH_3), 3.97–3.93 (d, 1H, $J = 13.4$ Hz), 3.84–3.97 (d, 1H, $J = 13.2$ Hz), 4.2–4.1 (d, 1H, $J = 10.4$ Hz), 7.3 (dd, 2H, thiophene-H), 7.4–7.2 (m, 5H, aro-

matic-H) ppm; FABMS m/z 364.10, calcd for $C_{19}H_{23}ClNO_2S$ (M-Cl)⁺, 364.11. Anal. ($C_{19}H_{23}Cl_2NO_2S$) C, H, N, Cl.

4.3.2.18. (±)-threo-N-(2-Methylpyridine)methylphenidate-2HCl (18). Using the same method as in the synthesis of **14**, a mixture of (±)-threo-methylphenidate (89 mg, 0.38 mmol) and 2-chloromethylpyridine (66 mg, 0.4 mmol) gave the titled compound. The dihydrochloride salt showed: mp 153–154 °C; ¹H NMR (CDCl₃): δ 1.6–1.1 (m, 6H), 2.58–2.53 (m, 1H), 3.03–2.95 (m, 1H), 3.66–3.49 (m, 1H), 3.69 (s, 3H, OCH₃), 3.96–3.91 (d, 1H, $J = 13.4$ Hz), 3.79–3.75 (d, 1H, $J = 13.2$ Hz), 4.18–4.14 (d, 1H, $J = 10.4$ Hz), 7.1 (t, 1H, pyridyl-H), 7.3–7.2 (m, 9H, aromatic-H), 7.4 (d, 1H, pyridyl-H), 7.8 (t, 1H, pyridyl-H), 8.45 (d, 1H, pyridyl-H) ppm; FABMS m/z 325.20, calcd for $C_{20}H_{25}N_2O_2$ (M-HCl-Cl)⁺, 325.19. Anal. ($C_{20}H_{26}Cl_2N_2O_2$) C, H, N, Cl.

4.3.2.19. (±)-threo-N-(3-Methylpyridine)methylphenidate-2HCl (19). Using the same method as in the synthesis of **14**, a mixture of (±)-threo-methylphenidate (89 mg, 0.38 mmol) and 3-chloromethylpyridine (66 mg, 0.4 mmol) gave the titled compound. The dihydrochloride salt showed: mp 159–160 °C; ¹H NMR (CDCl₃): δ 1.6–1.1 (m, 6H), 2.58–2.53 (m, 1H), 3.03–2.95 (m, 1H), 3.66–3.49 (m, 1H), 3.69 (s, 3H, OCH₃), 3.96–3.91 (d, 1H, $J = 13.4$ Hz), 3.79–3.75 (d, 1H, $J = 13.2$ Hz), 4.18–4.14 (d, 1H, $J = 10.4$ Hz), 7.3–7.2 (m, 9H, aromatic-H), 7.4 (s, 1H, pyridyl-H), 7.6 (d, 1H, pyridyl-H), 8.5 (d, 2H, pyridyl-H) ppm; FABMS m/z 325.20, calcd for $C_{20}H_{25}N_2O_2$ (M-HCl-Cl)⁺, 325.19. Anal. ($C_{20}H_{26}Cl_2NO_2$) C, H, N, Cl.

4.3.2.20. (±)-threo-N-(4-Methylpyridine)methylphenidate-2HCl (20). Using the same method as in the synthesis of **14**, a mixture of methylphenidate (89 mg, 0.38 mmol) and 4-pyridylmethylchloride (66 mg, 0.4 mmol) gave the titled compound. The dihydrochloride salt showed: mp 153–154 °C; ¹H NMR (CDCl₃): δ 1.60–1.10 (m, 6H), 2.58–2.53 (m, 1H), 3.03–2.95 (m, 1H), 3.66–3.49 (m, 1H), 3.69 (s, 3H), 3.79–3.75 (d, 1H, $J = 13.4$ Hz), 3.96–3.91 (d, 1H, $J = 13.4$ Hz), 4.18–4.14 (d, 1H, $J = 10.4$ Hz), 7.10 (t, 1H), 7.30–7.20 (m, 9H) ppm; FABMS m/z 325.20, calcd for $C_{20}H_{25}N_2O_2$ (M-HCl-Cl)⁺, 325.19. Anal. ($C_{20}H_{26}Cl_2NO_2$) C, H, N, Cl.

4.3.2.21. (±)-threo-N-(2-Methylfuran)methylphenidate-HCl (21). A mixture of (±)-threo-methylphenidate hydrochloride (0.260 g, 0.96 mmol) and 2-furaldehyde (0.125 g, 0.11 mL, 1.3 mmol) was dissolved in methanol (25 mL) followed by the addition of Et₃N (0.4 g). Into the solution was added 4 Å molecular sieves (4 g), and the reaction mixture stirred at room temperature for 1.5 h. NaBH₃CN (0.15 g, 2.38 mmol) was added into the solution, and the reaction was continued for an additional 18 h. The mixture was filtered and the filtrate and the washings were evaporated in vacuo. The residue was chromatographed on 10 g of silica gel using CHCl₃/MeOH (25:1) to give 110 mg (88%, pure by TLC analysis) titled compound. The hydrochloride salt showed: mp 170–171 °C; ¹H NMR (CDCl₃): δ 1.6–1.1 (m, 6H), 2.58–2.53 (m, 1H), 3.03–2.95 (m, 1H), 3.66–3.49 (m, 1H), 3.71 (s, 3H, OCH₃), 3.97–3.93 (d, 1H, $J = 13.4$ Hz), 3.84–3.97 (d, 1H, $J = 13.2$ Hz), 4.2–4.1 (d, 1H, $J = 10.4$ Hz), 6.4 (d, 1H, furan-H), 6.6 (d, 1H, furan-H), 7.4–7.2 (m, 5H, aromatic-H), 7.58 (d, 1H, furan-H) ppm; FABMS m/z 314.20, calcd for $C_{19}H_{24}NO_3$ (M-Cl)⁺, 314.18. Anal. ($C_{19}H_{24}ClNO_3$) C, H, N, Cl.

4.3.2.22. (±)-threo-N-(3-Methylthiophene)methylphenidate-HCl (22). Using the same method as in the synthesis of **21**, a mixture of (±)-threo-methylphenidate hydrochloride (0.260 g, 0.96 mmol) and thiophene-3-aldehyde (0.146 g, 0.11 mL, 1.3 mmol) gave the hydrochloride salt which showed: mp 175–176 °C; ¹H NMR (CDCl₃): δ 1.6–1.1 (m, 6H), 2.58–2.53 (m, 1H), 3.03–2.95

(m, 1H), 3.66–3.49 (m, 1H), 3.71 (s, 3H, OCH₃), 3.97–3.93 (d, 1H, $J = 13.4$ Hz), 3.84–3.97 (d, 1H, $J = 13.2$ Hz), 4.2–4.1 (d, 1H, $J = 10.4$ Hz), 7.1 (s, 1H, thiophene-H), 7.4–7.2 (m, 5H, aromatic-H), 7.50 (d, 1H, thiophene-H), 7.60 (d, 1H, thiophene-H) ppm; FABMS m/z 330.17, calcd for $C_{19}H_{24}NO_2S$ (M-Cl)⁺, 330.15. Anal. ($C_{19}H_{24}ClNO_2S$) C, H, N, Cl.

4.3.2.23. (±)-threo-N-(2-Methylthiophene)methylphenidate-HCl (23). Using the same method as in the synthesis of **21**, a mixture of (±)-threo-methylphenidate hydrochloride (0.260 g, 0.96 mmol) and thiophene-2-aldehyde (0.146 g, 0.11 mL, 1.3 mmol) gave the hydrochloride salt which showed: mp 180–181 °C; ¹H NMR (CDCl₃): δ 1.6–1.1 (m, 6H), 2.58–2.53 (m, 1H), 3.03–2.95 (m, 1H), 3.66–3.49 (m, 1H), 3.71 (s, 3H, OCH₃), 3.97–3.93 (d, 1H, $J = 13.4$ Hz), 3.84–3.97 (d, 1H, $J = 13.2$ Hz), 4.2–4.1 (d, 1H, $J = 10.4$ Hz), 6.9 (d, 1H, thiophene-H), 7.3 (dd, 2H, thiophene-H), 7.4–7.2 (m, 5H, aromatic-H) ppm; FABMS m/z 330.16, calcd for $C_{19}H_{24}NO_2S$ (M-Cl)⁺, 330.15. Anal. ($C_{19}H_{24}ClNO_2S$) C, H, N, Cl.

4.3.2.24. (±)-threo-N-(3-Methylfuran)methylphenidate-HCl (24). Using the same method as in the synthesis of **21**, a mixture of methylphenidate (260 mg, 0.96 mmol) and 3-furaldehyde (125 mg, 1.3 mmol) gave the hydrochloride salt which showed: mp 181–182 °C; ¹H NMR (CDCl₃): δ 1.60–1.10 (m, 6H), 2.58–2.53 (m, 1H), 3.03–2.95 (m, 1H), 3.66–3.49 (m, 1H), 3.71 (s, 3H), 3.84–3.97 (d, 1H, $J = 13.4$ Hz), 3.97–3.93 (d, 1H, $J = 13.4$ Hz), 4.20–4.10 (d, 1H, $J = 10.4$ Hz), 6.40 (s, 1H), 6.60 (d, 1H), 7.40–7.20 (m, 5H), 7.50 (dd, 2H) ppm; FABMS m/z 314.20, calcd for $C_{19}H_{24}NO_3$ (M-Cl)⁺, 314.18. Anal. ($C_{19}H_{24}ClNO_3$) C, H, N, Cl.

4.3.2.25. (±)-threo-N-Ethylritalinol (25). Using the same method as in the synthesis of **2**, acetyl chloride gave a very viscous colorless liquid (140 mg, 69% based on methylphenidate). ¹H NMR (CDCl₃): δ 0.99 (m, 1H), 1.20 (t, 2H), 1.30–1.60 (m, 5H), 2.75–2.60 (t, 3H), 2.81–2.75 (t, 2H, N-CH₂), 3.2–3.1 (d, 1H), 3.35–3.20 (t, 1H), 3.40 (t, 1H), 3.79 (dd, 1H, from CH₂OH), 4.0 (t, 1H, from CH₂OH), 7.38–7.10 (m, 5H, aromatic-H) ppm; CIMS m/z 234.200, calcd for $C_{15}H_{24}NO$ (MH)⁺, 234.186. Anal. ($C_{15}H_{23}NO$) C, H, N.

4.3.2.26. (±)-threo-3',5'-Dimethylmethylphenidate-HCl (26). Using the same method as previously described,¹² 10.0 g of 3,5-dimethylphenylacetonitrile and 10.9 g of 2-bromopyridine gave 0.425 g of the HCl salt which showed: mp 229–230 °C. ¹H NMR (D₂O): δ 7.1 (s, 1H), 6.8 (s, 2H), 3.84 (d, 1H), 3.75–3.72 (m, 1H), 3.59 (s, 3H), 3.31–3.13 (m, 1H), 2.83–2.79 (m, 1H), 2.2 (s, 6H), 1.94–1.40 (m, 6H) ppm; CIMS m/z 262.18, calcd for $C_{16}H_{24}NO_2$ (M-Cl)⁺, 262.18. Anal. ($C_{16}H_{24}ClNO_2 \cdot 0.50H_2O$): C, H, N, Cl.

4.3.2.27. (±)-threo-3',5'-Dichloromethylphenidate-HCl (27). Using the same method as previously described,¹² 4.0 g of 3,5-dichlorophenylacetonitrile and 3.4 g of 2-bromopyridine gave 0.105 g of the HCl salt which showed: mp 198–200 °C. ¹H NMR (D₂O): δ 7.4 (s, 1H), 7.2 (s, 2H), 3.84 (d, 1H), 3.75–3.72 (m, 1H), 3.59 (s, 3H), 3.31–3.13 (m, 1H), 2.83–2.79 (m, 1H), 1.94–1.40 (m, 6H) ppm; CIMS m/z 302.06, calcd for $C_{14}H_{18}Cl_2NO_2$ (M-Cl)⁺, 302.07. Anal. ($C_{14}H_{18}Cl_2NO_2 \cdot 0.75H_2O$): C, H, N, Cl.

4.3.2.28. (±)-threo-N-3-Chlorobenzylmethylphenidate-HCl (28). Using the same method as in the synthesis of **14**, a mixture of methylphenidate (89 mg, 0.38 mmol) and 3-chlorobenzylchloride (82 mg, 0.40 mmol) gave the titled compound. The hydrochloride salt was recrystallized from EtOAc/hexane and showed: mp 179–180 °C; ¹H NMR (CDCl₃): δ 1.60–1.10 (m, 6H), 2.58–2.53 (m, 1H), 3.03–2.95 (m, 1H), 3.66–3.49 (m, 1H), 3.69 (s, 3H), 3.78–3.74 (d, 1H, $J = 13.3$ Hz), 3.96–3.91 (d, 1H, $J = 13.3$ Hz),

4.18–4.14 (d, 1H, $J = 10.2$ Hz), 7.40–7.20 (m, 9H) ppm; CIMS m/z 358.160, calcd for $C_{21}H_{25}ClNO_2$ ($M-Cl$)⁺, 358.157. Anal. ($C_{21}H_{25}Cl_2NO_2$) C, H, N, Cl.

4.3.2.29. (±)-threo-Ritalinol (30). Using the same procedure as in the synthesis of **61**, methylphenidate (1.61 g, 6.91 mmol) gave the pure product as a white solid (mp 95.4–97 °C, 0.95 g, 99%). ¹H NMR ($CDCl_3$): δ 7.35–7.20 (m, 5H), 3.99–3.93 (dd, 1H), 3.88–3.83 (dd, 1H), 3.11–3.06 (m, 1H), 2.97–2.90 (q, 1H), 2.67–2.55 (m, 2H), 1.80–1.76 (m, 1H), 1.63–1.59 (m, 1H), 1.45–1.21 (m, 3H) ppm. CIMS m/z 206.159, calcd for $C_{13}H_{20}NO$ (MH)⁺, 206.155. Anal. ($C_{13}H_{19}NO$) C, H, N.

4.3.2.30. (±)-threo-4-Hydroxy-N-methylmethylphenidate (33) and by-product (32). A 200 mg sample of **39** was converted to the free base, and mixed with 1 mL of 37% formaldehyde and 1 mL of HCO_2H . After heating under reflux for 2 h, the mixture was evaporated, taken up in EtOAc, washed with $NaHCO_3$ solution and the organic layer was dried and evaporated. This gave 225 mg of a clear oil which was carefully chromatographed on silica gel using EtOAc/MeOH (90:10). This gave 57 mg of **33** and 28 mg of **32**. Compound **33**: ¹H NMR ($CDCl_3$): δ 7.3 (s, 1H), 7.2 (d, 2H), 6.7 (d, 2H), 3.83 (d, $J = 9.9$ Hz, 1H), 3.68 (s, 3H), 3.22–3.1 (m, 1H), 3.05–2.9 (m, 1H), 2.6–2.5 (m, 1H), 2.4 (s, 3H), 1.8–1.0 (m, 6H) ppm. Anal. ($C_{15}H_{21}NO_3$): C, H, N. Compound **32**: ¹H NMR ($CDCl_3$): δ 7.1 (d, 1H), 6.95 (s, 1H), 6.8 (s, 1H), 5.25 (s, 2H), 4.9 (s, 1H), 3.77 (d, $J = 9.9$ Hz, 1H), 3.68 (s, 3H), 3.1 (m, 1H), 2.95 (m, 1H), 2.55 (m, 1H), 2.4 (s, 3H), 1.6–1.0 (m, 6H) ppm. Anal. ($C_{17}H_{25}NO_5$): C, H, N.

4.3.2.31. (±)-threo-3-Fluororitalinol (60). Using the same procedure as in the synthesis of **61**, **57** (103 mg, 0.36 mmol) afforded **60** as a white solid after recrystallization from ether (48 mg, 60%) which showed: mp 98–99 °C. ¹H NMR ($CDCl_3$): δ 7.28 (dd, 1H, $J = 14.0, 8.2$ Hz), 7.1–6.9 (m, 3H), 3.95 (dd, 1H), 3.85 (dd, 1H), 3.09–3.00 (m, 1H), 2.93 (q, 1H), 2.65–2.52 (m, 2H), 1.76 (m, 1H), 1.60–1.57 (m, 1H), 1.40–1.20 (m, 3H) ppm. Anal. ($C_{13}H_{18}FNO$): C, H, N.

4.3.2.32. (±)-threo-3',4'-Dichlororitalinol (61). To the solution of 3',4'-dichloromethylphenidate (162 mg, 0.54 mmol) in ether (15 mL) was added 1 M lithium aluminum hydride (4.5 mL, 4.5 mmol) via syringe at 0 °C under a nitrogen atmosphere. The solution was stirred at 0 °C for 2 h and water carefully added drop by drop until no gas was evolved. The ether was washed with water three times and then dried ($MgSO_4$). Evaporation of the solvent gave a white solid that proved to be the pure product **61** (mp 134–136 °C, 146 mg, 99%). ¹H NMR ($CDCl_3$): δ 7.38 (d, 1H, $J = 8.2$ Hz), 7.33 (d, 1H, $J = 2.2$ Hz), 7.08 (dd, 1H, $J = 2.2, 8.2$ Hz), 3.97 (dd, 1H, $J = 7.7$ Hz, 11.0 Hz), 3.86 (dd, 1H, $J = 3.7, 11.0$ Hz), 3.11–3.06 (m, 1H), 2.97–2.90 (m, 1H), 2.67–2.55 (m, 2H), 1.80–1.76 (m, 1H), 1.63–1.59 (m, 1H), 1.45–1.21 (m, 3H) ppm; CIMS m/z 274.07, calcd for $C_{13}H_{18}Cl_2NO$ (MH)⁺, 274.08; HCl salt, mp 164–167 °C (dec). Anal. ($C_{13}H_{18}Cl_3NO \cdot 0.40 H_2O$) C, H, N, Cl.

4.3.2.33. (±)-threo-3',4'-Dichlororitalinol methyl ether-HCl (62). A mixture of **52** (185 mg, 0.55 mmol), chloroform (10 mL), water (5 mL), $NaHCO_3$ (105 mg), NaCl (120 mg) and $(BOC)_2O$ (128 mg, 0.59 mmol) was heated under a gentle reflux for 90 min. The chloroform layer was washed with ice-cold HCl (1 N, 10 mL) and then water (3 \times 10 mL), and dried ($MgSO_4$) to give a colorless oil (270 mg, 111%). To the solution of the *N*-BOC ester in anhydrous diethyl ether (8 mL) was added lithium aluminum hydride (0.6 mL, 0.6 mmol, 1.0 M in ether solution) via syringe at 0 °C under a nitrogen atmosphere. The solution was then stirred at 0 °C for 1 h and then at rt for 25 min. Water was added dropwise

very slowly and the ether was washed with water and dried ($MgSO_4$). The solvent was removed to give the *N*-BOC alcohol as a colorless oil (233 mg, 96% in two steps). Dry DMSO (23 mL) was added to ground KOH (490 mg) and the suspension was stirred at rt under a nitrogen atmosphere for 20 min. The *N*-BOC alcohol (610 mg) was dissolved in DMSO (15 mL) and added into the KOH/DMSO mixture in one portion, followed by immediate addition of CH_3I (0.57 mL). The mixture was stirred at rt overnight and then diluted by methylene chloride (150 mL), washed with water (5 \times 30 mL), and dried ($MgSO_4$) to give a pale yellow oil (565 mg) after evaporation of the solvent. The crude product was then purified using silica gel column chromatography (5% EtOAc/hexane followed by 10% EtOAc/hexane) to give the pure BOC-protected methyl ether product as a colorless oil (251 mg, 46% in two steps). ¹H NMR ($CDCl_3$): δ 7.41–7.11 (m, 3H), 4.47–4.31 (m, 1H), 4.19–3.98 (m, 1H), 3.59–3.45 (m, 2H), 3.38–3.31 (m, 1H), 3.22 (s, 3H), 2.89–2.81 (m, 1H), 1.66–1.25 (m, 15H) ppm. The BOC-protected methyl ether (250 mg, 0.68 mmol) was mixed with trifluoroacetic acid (3.5 mL) and stirred at rt for 30 min. The TFA was then evaporated to give a pale yellow oil (360 mg). The oil was then dissolved in EtOAc and washed with 5% sodium carbonate and dried ($MgSO_4$). A colorless oil (153 mg) was obtained as the pure product (**4d**) (83%) after evaporation of the solvent. ¹H NMR ($CDCl_3$): δ 7.37 (d, 1H, $J = 8.2$ Hz), 7.31 (s, 1H), 7.07–7.04 (dd, 1H, $J = 1.7, 8.2$ Hz), 3.67 (d, 2H, $J = 8.2$ Hz), 3.32 (s, 3H), 3.09 (d, 1H, $J = 12.1$ Hz), 2.79–2.75 (m, 2H), 2.63 (t, 1H, $J = 9.3$ Hz), 2.07 (br s, 1H), 1.73–0.99 (m, 6H) ppm. The free base was converted to its HCl salt which showed: mp 202–205 °C, ¹H NMR (D_2O): δ 7.41 (d, 1H, $J = 8.2$ Hz), 7.35 (s, 1H), 7.06 (d, 1H, $J = 8.2$ Hz), 3.73 (t, 1H), 3.60–3.5 (m, 1H), 3.38 (t, 1H), 3.29–3.15 (m, 4H), 3.07–3.04 (q, 1H), 2.86 (t, 1H), 1.67–1.18 (m, 6H) ppm. Anal. ($C_{14}H_{20}Cl_3NO \cdot 0.50 H_2O$) C, H, N, Cl.

4.3.2.34. (±)-threo-N-Benzyl-3'-chloromethylphenidate-HCl (63). Using the same procedure as in the synthesis of **7**, 3'-chloromethylphenidate (49 mg, 0.16 mmol) and benzylbromide afforded **63** as a off-white solid (mp 86.4–87.9 °C, 39.7 mg, 69%); ¹H NMR ($CDCl_3$): δ 7.42–7.21 (m, 9H), 4.15 (d, 1H, $J = 11.6$ Hz), 3.94 (d, 1H, $J = 13.7$ Hz), 3.79 (d, 1H, $J = 13.2$ Hz), 3.67 (s, 3H), 3.50–3.44 (m, 1H), 2.96–2.91 (m, 1H), 2.58–2.52 (m, 1H), 1.58–1.05 (m, 6H) ppm. The HCl salt showed mp 116–162 °C (dec). Anal. ($C_{21}H_{24}ClNO_2$) C, H, N, Cl.

4.3.2.35. (±)-threo-N-Benzylmethylphenidate dimethyl amide-HCl (64). Using the same procedures as in the synthesis of **65** (using dimethyl amine and 60 mg of *N*-benzylritalinic acid), the pure amide was obtained as a pale yellow solid (mp 110–111 °C, 45 mg, 74%). ¹H NMR ($CDCl_3$): δ 7.41–7.20 (m, 10H), 4.18 (d, 1H, $J = 9.9$ Hz), 3.75–3.68 (m, 3H), 2.95 (d, 6H, $J = 15$ Hz), 2.75–2.73 (m, 1H), 2.48–2.43 (m, 1H), 1.69–1.07 (m, 6H) ppm; EIMS m/z 337.221, calcd for $C_{22}H_{29}N_2O$ (MH)⁺, 337.228. The HCl salt showed mp 201 °C (dec). Anal. ($C_{22}H_{29}ClN_2O \cdot 0.25H_2O$): C, H, N, Cl.

4.3.2.36. (±)-threo-N-Benzylmethylphenidate amide-HCl (65). *N*-Benzylmethylphenidate (**29**) (400 mg, 1.24 mmol) was mixed with 6 N HCl (2.5 mL) and the solution was heated under reflux for 1 h. The solvent was removed to afford *N*-benzylritalinic acid as a white solid (426 mg, 99.5%) which showed mp 121–160 °C. ¹H NMR δ 7.40–7.09 (m, 10H), 4.61 (d, 1H, $J = 13.2$ Hz), 4.39–4.30 (m, 2H), 4.03–3.80 (m, 1H), 3.50–3.33 (m, 1H), 3.21–3.06 (m, 1H), 1.92–1.01 (m, 6H) ppm. The acid (84 mg, 0.24 mmol) was suspended in chloroform (3 mL) at room temperature. A few drops of DMF were added and followed with the addition of thionyl chloride (0.1 mL). The suspension changed to a clear solution after a few minutes and then was cooled via ice-bath. This cooled solution

was then added to a concentrated ammonium hydroxide solution (4 mL) dropwise at 0 °C and the resulting mixture was stirred at 0 °C for 10 min and then rt for 2 h. The organic layer was separated and the aqueous layer was extracted with chloroform (2 × 10 mL). The combined organic layers were washed with water (2 × 10 mL) and dried (MgSO₄). After removal of the solvent, a yellow solid was obtained (79.3 mg). The crude product was purified by silica gel column chromatography (1:1 EtOAc/hexane) to give the pure product as a yellow solid (mp 134–135 °C, 24 mg, 32%). ¹H NMR (CDCl₃): δ 7.88 (br s, 1H), 7.36–7.22 (m, 10H), 5.52 (br s, 1H), 3.92–3.79 (m, 3H), 3.44–3.37 (m, 1H), 2.98–2.90 (m, 1H), 2.60–2.54 (m, 1H), 1.75–1.41 (m, 5H), 1.26–1.16 (m, 1H) ppm. EIMS *m/z* 309.198, calcd for C₂₀H₂₅N₂O (MH)⁺, 309.197. HCl salt mp 157–180 °C (dec). Anal. (C₂₀H₂₅ClN₂O·0.60 H₂O), C, H, N, Cl.

4.3.2.37. (±)-threo-Ritalinol methyl ether-HCl (68). The HCl salt of **67**, (68 mg, 0.20 mmol) was dissolved in methanol (5 mL) and palladium hydroxide (20 mg, 20% Pd, wet) was then added. Hydrogenation was carried out at 45 psi for 2 h. The catalyst was filtered off and the solvent was removed to afford pure **68** as a white solid (mp 154–155 °C, 50 mg, 99%). ¹H NMR (D₂O): δ 7.32–7.14 (m, 5H), 3.76 (dd, 1H, *J* = 8.2, 9.9 Hz), 3.73 (dd, 1H, *J* = 6.0, 9.9 Hz), 3.43–3.37 (m, 1H), 3.23–3.21 (m, 4H), 3.10–3.03 (m, 1H), 2.91–2.82 (m, 1H), 1.65–1.17 (m, 6H) ppm. Anal. (C₁₄H₂₂ClNO·0.50 H₂O): C, H, N, Cl.

4.3.2.38. (±)-threo-N-Benzyl-3',4'-dichloromethylphenidate-HCl (69). Using the same procedure as in the synthesis of **7**, 3',4'-dichloromethylphenidate (360 mg, 1.1 mmol) and excess benzyl bromide afforded **69** as a pale yellow solid (mp 94.7–95.8 °C, 348 mg, 84%). ¹H NMR (CDCl₃): δ 7.52 (d, 1H, *J* = 2.2 Hz), 7.39 (d, 1H, *J* = 8.3 Hz), 7.34–7.23 (m, 6H), 4.13 (d, 1H, *J* = 11.5 Hz), 3.93 (d, 1H, *J* = 13.7 Hz), 3.78 (d, 1H, *J* = 13.7 Hz), 3.67 (s, 3H), 3.44 (d, 1H, *J* = 11.0 Hz), 2.98–2.90 (dt, 1H), 2.57–2.51 (m, 1H), 1.57–1.52 (m, 4H), 1.49–1.32 (m, 1H), 1.06–1.04 (m, 1H) ppm; EIMS *m/z* 392.114, calcd for C₂₁H₂₄Cl₂NO₂ (MH)⁺, 392.118. HCl salt, mp 116–162 °C (dec). Anal. (C₂₁H₂₄Cl₂NO₂) C, H, N, Cl.

4.3.2.39. (±)-threo-N-Benzyl-3',4'-dichlororitalinol-HCl (70). Using the same procedure as in the synthesis of **61**, **69** (618 mg, 1.58 mmol) afforded a colorless oil as pure **70** (601 mg, 95%). ¹H NMR (CDCl₃): δ 7.34–7.23 (m, 6H), 7.07 (d, 1H, *J* = 2.2 Hz), 6.81 (dd, 1H, *J* = 2.2, 8.3 Hz), 3.90 (s, 3H), 3.68 (t, 1H, *J* = 11.0 Hz), 3.58 (dd, 1H, *J* = 3.9, 11.0 Hz), 3.35 (dt, 1H, *J* = 3.3, 11.5 Hz), 3.19–3.02 (m, 2H), 2.69–2.64 (m, 1H), 1.75–1.44 (m, 4H), 1.30–1.27 (m, 1H), 0.88–0.83 (m, 1H) ppm. The HCl salt showed: mp 215 °C (dec); ¹H NMR (D₂O): δ 7.47–7.36 (m, 7H), 7.14–7.11 (d, 1H, *J* = 8.2 Hz), 4.77–4.62 (m, 1H), 4.41–4.26 (m, 1H), 4.03–3.62 (m, 4H), 3.45–3.38 (m, 1H), 3.08–2.96 (m, 1H), 1.95–1.32 (m, 6H) ppm; Anal. (C₂₀H₂₄Cl₂NO): C, H, N, Cl.

4.3.2.40. (±)-threo-N-Benzyl-3',4'-dichlororitalinol methyl ether-HCl (71). To 3 mL of DMSO was added KOH (68 mg, powder, 1.21 mmol). After stirring for 20 min at rt, **70** (120 mg, 0.4 mmol) in DMSO (3 mL) was added in one portion, followed immediately by methyl iodide (45 μL, 0.73 mmol). The mixture was stirred at rt for 24 h and methylene chloride (60 mL) was added; after washing with water, the organic layer was dried, filtered and evaporated to give 104 mg of a white solid (mp 74–76 °C, 83%). ¹H NMR (CDCl₃): δ 7.36–7.23 (m, 7H), 7.03 (dd, 1H, *J* = 2.2, 8.2 Hz), 3.95 (d, 1H, *J* = 13.7 Hz), 3.88 (dd, 1H, *J* = 3.4, 9.3 Hz), 3.75 (d, 1H, *J* = 13.7 Hz), 3.60 (t, 1H, *J* = 9.3 Hz), 3.38 (dt, 1H, *J* = 3.4, 9.5 Hz), 3.28 (s, 3H), 2.98–2.89 (m, 1H), 2.83–2.76 (m, 1H), 2.52–2.44 (m, 1H), 1.67–1.26 (m, 5H), 1.07–1.02 (m, 1H) ppm; EIMS *m/z* 378.133, calcd for C₂₁H₂₆Cl₂NO (MH)⁺, 378.139. HCl salt mp 202–204 °C. Anal. (C₂₁H₂₆Cl₂NO): C, H, N, Cl.

4.3.2.41. (±)-threo-3',4'-Dichloromethylphenidate amide-HCl (72). Using the same method as previously described,¹² 30.4 g of 3,4-dichlorophenylacetonitrile and 21.5 g of 2-bromopyridine gave 15.6 g of the crude amide (third intermediate) as an *erythro/threo* mixture (2:1). A 200 mg portion was carefully chromatographed on silica gel using EtOAc/MeOH/Et₂NH (10:90:0.1). This gave 54 mg of the *threo* isomer which was converted to the HCl salt and crystallized from MeOH/Ether (39 mg). The HCl salt showed: mp 251–253 °C; ¹H NMR (CDCl₃): δ 8.1 (br s, 1H), 7.40 (d, 1H, *J* = 8.2 Hz), 7.45 (s, 1H), 7.04 (d, 1H, *J* = 8.2 Hz), 5.62 (br s, 1H), 3.92–3.79 (m, 3H), 3.44–3.37 (m, 1H), 2.98–2.90 (m, 1H), 2.60–2.54 (m, 1H), 1.75–1.41 (m, 5H), 1.26–1.16 (m, 1H) ppm. CIMS *m/z* 287.074, calcd for C₁₃H₁₇Cl₂N₂O (M–Cl)⁺, 287.072. Anal. (C₁₃H₁₇Cl₂N₂O·0.75 H₂O): C, H, N, Cl.

4.3.2.42. (±)-threo-Benzylphenidate-HCl (73). Methylphenidate (**39**) (190 mg, 0.70 mmol) was mixed with 6 N HCl (2.5 mL) and the solution was heated under reflux for 1 h. The solvent was removed to afford a white solid (ritalinic acid) which was mixed with 5 mL of benzyl alcohol at 90 °C for 3 h. After cooling to rt, 40 mL of ether was added, the solid material removed and the filtrate concentrated to give white crystals (65 mg), mp 194–196 °C. ¹H NMR (CDCl₃): δ 1.6–1.1 (m, 6H), 2.58–2.53 (m, 1H), 3.03–2.95 (m, 1H), 3.66–3.49 (m, 1H), 4.2–4.1 (d, 1H, *J* = 10.4 Hz), 4.95 (d, 1H, *J* = 13.4 Hz), 4.90 (d, 1H, *J* = 13.4 Hz), 7.4–7.2 (m, 10H) ppm. Anal. (C₂₀H₂₄ClNO₂): C, H, N, Cl.

4.3.2.43. (±)-threo-N-Methyl-3'-methylmethylphenidate (74). A 100 mg sample of **59** was converted to the free base, dissolved in 2 mL of MeOH and 40 μL of 37% formaldehyde, 10 μL of HOAc and 20 mg of 5% Pd/C added. After 2 h of H₂ treatment at 40 psi, the mixture was filtered and evaporated, taken up in EtOAc, dried and evaporated again. This gave 74 mg of a clear oil. ¹H NMR (CDCl₃): δ 7.2–7.1 (m, 4H), 3.83 (d, *J* = 9.9 Hz, 1H), 3.68 (s, 3H), 3.22–3.1 (m, 1H), 3.05–2.9 (m, 1H), 2.6–2.5 (m, 1H), 2.4 (s, 3H), 1.8–1.0 (m, 6H) ppm. Anal. (C₁₆H₂₃NO₂): C, H, N.

4.3.2.44. (±)-threo-Ritalinol acetate (75). A 355 mg portion of **30**-HCl was mixed with excess acetyl chloride. After 2 h the mixture was evaporated, added to acetone and activated C, stirred for 3 h, filtered and evaporated. The crude product (250 mg) was converted to the free base and it was crystallized first from acetone and then EtOAc/hexane to give 52 mg of white solid (mp 116–117 °C). ¹H NMR (CDCl₃): δ 7.4–7.2 (m, 5H), 5.08 (d, 1H, *J* = 12.1 Hz), 3.78–3.64 (m, 3H), 3.55 (d, 1H, *J* = 11.4 Hz), 3.06 (d, 1H, *J* = 12.1 Hz), 2.24 (s, 3H), 1.8–1.3 (m, 6H) ppm. Anal. (C₁₅H₂₁NO₂) C, H, N.

4.3.2.45. (±)-threo-Methylphenidate amide (76). Using exactly the same procedure as described in the synthesis of **72**, 29.4 g of phenylacetonitrile and 39.5 g of 2-bromopyridine gave 19.4 g of the crude amide (fourth intermediate, after epimerization) as an *threo/erythro* mixture (9:1). A 230 mg portion of the free base was carefully crystallized from EtOAc to yield 194 mg of the pure *threo* isomer which showed mp 174–176 °C; ¹H NMR (CDCl₃): δ 7.8 (br s, 1H), 7.4–7.2 (m, 5H), 5.71 (br s, 1H), 3.9–3.8 (m, 3H), 3.49–3.44 (m, 1H), 2.95–2.90 (m, 1H), 2.59–2.54 (m, 1H), 1.71–1.45 (m, 5H), 1.21–1.16 (m, 1H) ppm; EIMS *m/z* 218.149, calcd for C₁₃H₁₈N₂O (M)⁺, 218.142. Anal. (C₁₃H₁₈N₂O): C, H, N.

4.3.2.46. (±)-threo-4'-Ethylmethylphenidate-HCl (78). Using the same method as previously described,¹² 5.0 g of 4-ethylphenylacetonitrile and 5.4 g of 2-bromopyridine gave 0.39 g of the HCl salt which showed: mp 204–205 °C; ¹H NMR (D₂O): δ 7.28 (d, 2H), 7.08 (d, 2H), 3.80 (d, *J* = 9.4 Hz, 1H), 3.64 (m, 1H), 3.58 (s, 3H), 3.30 (m, 1H), 2.93 (m, 1H), 2.92 (q, 2H), 1.8–1.2 (m, 6H),

1.02 (t, 3H) ppm; CIMS m/z 262.180, calcd for $C_{16}H_{24}NO_2$ ($M-Cl$)⁺, 262.181. Anal. ($C_{16}H_{24}ClNO_2 \cdot 0.25 H_2O$): C, H, N, Cl.

Acknowledgments

This work was supported in part by NIH grants DA06305 (M.M.S. and H.M.D.), DA11541 (H.M.D., M.M.S., and C.A.V.) and DA018153 (C.A.V.). M.M.S. gratefully acknowledges the technical assistance of Mr. Adam Eason, Ms. Monica Stafford, Ms. LeKeisha Nelson, and Mr. Eric Shields.

Supplementary data

Supplementary data (predicted pIC_{50} 's and associated residuals for the training set for the 2D- and 3D-QSAR models and the elemental analysis data for the analogs) associated with this article can be found, in the online version, at [doi:10.1016/j.bmc.2010.08.034](https://doi.org/10.1016/j.bmc.2010.08.034).

References and notes

- Kuhar, M. J.; Ritz, M. C.; Boja, J. W. *Trends Neurosci.* **1991**, *14*, 299.
- Giros, B.; Jaber, M.; Jones, S. R.; Wightman, R. M.; Caron, M. G. *Nature* **1996**, *379*, 606.
- Chen, N. H.; Reith, M. E. In *Contemporary Neuroscience: Neurotransmitter Transporters: Structure, Function, and Regulation*; Reith, M. E. A., Ed.; Humana Press: Totowa, NJ, 1997; p 53.
- Singh, S. *Chem. Rev.* **2000**, *100*, 925.
- Carroll, F. I. *J. Med. Chem.* **2003**, *46*, 1775.
- Prisinzano, T.; Rice, K. C.; Baumann, M. H.; Rothman, R. B. *Curr. Med. Chem. (CNSA)* **2004**, *4*, 47.
- Gatley, S. J.; Pan, D.; Chen, R.; Chaturvedi, G.; Ding, Y. S. *Life Sci.* **1996**, *58*, PL 231.
- Kim, D.-I.; Deutsch, H. M.; Ye, X.; Schweri, M. M. *J. Med. Chem.* **2007**, *50*, 2718.
- Reith, M. E. A. *NIDA Res. Monogr.* **1988**, *88*, 23.
- Schweri, M. M.; Skolnick, P.; Rafferty, M. F.; Rice, K. C.; Janowsky, A. J.; Paul, S. M. *J. Neurochem.* **1985**, *45*, 1062.
- Schweri, M. M. *Neuropharmacology* **1990**, *29*, 901.
- Deutsch, H. M.; Shi, Q.; Gruszecka-Kowalik, E.; Schweri, M. M. *J. Med. Chem.* **1996**, *39*, 1201.
- Froimowitz, M.; Deutsch, H. M.; Shi, Q.; Wu, K.-M.; Glaser, R.; Adin, I.; George, C.; Schweri, M. M. *Bioorg. Med. Chem. Lett.* **1997**, *7*, 1213.
- Glaser, R.; Adin, I.; Shifftan, D.; Shi, Q.; Deutsch, H. M.; George, C.; Wu, K.-M.; Froimowitz, M. *J. Org. Chem.* **1998**, *63*, 1785.
- Deutsch, H. M. *Med. Chem. Res.* **1998**, *8*, 91.
- Wayment, H. K.; Deutsch, H. M.; Schweri, M. M.; Schenk, J. O. *J. Neurochem.* **1999**, *72*, 1266.
- Deutsch, H. M.; Ye, X.; Shi, Q.; Liu, Z.; Schweri, M. M. *Eur. J. Med. Chem.* **2001**, *36*, 303.
- Deutsch, H. M.; Kim, D. I.; Holtzman, S. G.; Schweri, M. M.; Spelman, R. D. In *College on the Problems of Drug Dependence, 64th Annual Meeting*; Quebec City, Canada, 2002.
- Schweri, M. M.; Deutsch, H. M.; Massey, A. T.; Holtzman, S. G. *J. Pharmacol. Exp. Ther.* **2002**, *301*, 527.
- Davies, H. M. L.; Hopper, D. W.; Hansen, T.; Liu, Q.; Childers, S. R. *Bioorg. Med. Chem. Lett.* **2004**, *14*, 1799.
- Froimowitz, M.; Gu, Y.; Dakin, L. A.; Nagafuji, P. M.; Kelley, C. J.; Parrish, D.; Deschamps, J. R.; Janowsky, A. J. *J. Med. Chem.* **2007**, *50*, 219.
- Patrick, K. S.; Williard, R. L.; VanWert, A. L.; Dowd, J. J.; Oatis, J. E., Jr.; Middaugh, L. D. *J. Med. Chem.* **2005**, *48*, 2876.
- Froimowitz, M.; Gu, Y.; Dakin, L. A.; Kelley, C. J.; Parrish, D.; Deschamps, J. R. *Bioorg. Med. Chem. Lett.* **2005**, *15*, 3044.
- Froimowitz, M.; Patrick, K. S.; Cody, V. *Pharm. Res.* **1995**, *12*, 1430.
- Giros, B.; El Mestikawy, S.; Bertrand, L.; Caron, M. G. *FEBS Lett.* **1991**, *295*, 149.
- Gilbert, K. M.; Skawinski, W. J.; Misra, M.; Paris, K. A.; Naik, N. H.; Buono, R. A.; Deutsch, H. M.; Venanzi, C. A. *J. Comput. Aided Mol. Des.* **2004**, *18*, 719.
- Maw, H. H.; Hall, L. H. *J. Chem. Inf. Comput. Sci.* **2000**, *40*, 1270.
- Hoffman, B. T.; Kopajtic, T.; Katz, J. L.; Newman, A. H. *J. Med. Chem.* **2000**, *43*, 4151.
- Christensen, H. S.; Boye, S. V.; Thinggaard, J.; Sinning, S.; Wiborg, O.; Schiott, B.; Bols, M. *Bioorg. Med. Chem.* **2007**, *15*, 5262.
- Carroll, F. I.; Gao, Y.; Rahman, M. A.; Abrams, P.; Parham, K.; Lewin, A. H.; Boja, J. W.; Kuhar, M. J. *J. Med. Chem.* **1991**, *34*, 2719.
- Carroll, F. I.; Mascarella, S. W.; Kuzemko, M. A.; Gao, Y.; Abraham, P.; Lewin, A. H.; Boja, J. W.; Kuhar, M. J. *J. Med. Chem.* **1994**, *37*, 2865.
- Lieske, S. F.; Yang, B.; Eldefrawi, M. E.; MacKerell, A. D., Jr.; Wright, J. J. *Med. Chem.* **1998**, *41*, 864.
- Muszynski, I. C.; Scapozza, L.; Kovar, K.-A.; Folkers, G. *Quant. Struct.-Act. Relat.* **1999**, *18*, 342.
- Zhu, N.; Harrison, A.; Trudell, M. L.; Klein-Stevens, C. L. *Struct. Chem.* **1999**, *10*, 91.
- Davies, H. M. L.; Gilliatt, V.; Kuhn, L. A.; Saikali, E.; Ren, P.; Hammond, P. S.; Sexton, G. J.; Childers, S. R. *J. Med. Chem.* **2001**, *44*, 1509.
- Yuan, H.; Kozikowski, A. P.; Petukhov, P. A. *J. Med. Chem.* **2004**, *47*, 6137.
- Yuan, H.; Petukhov, P. A. *Bioorg. Med. Chem. Lett.* **2006**, *16*, 6267.
- Newman, A. H.; Izenwasser, S.; Robarge, M. J.; Kline, R. H. *J. Med. Chem.* **1999**, *42*, 3502.
- Robarge, M. J.; Agoston, G. E.; Izenwasser, S.; Kopajtic, T.; George, C.; Katz, J. L.; Newman, A. H. *J. Med. Chem.* **2000**, *43*, 1085.
- Kulkarni, S. S.; Grundt, P.; Kopajtic, T.; Katz, J. L.; Newman, A. H. *J. Med. Chem.* **2004**, *47*, 3388.
- Kulkarni, S. S.; Newman, A. H.; Houlihan, W. J. *J. Med. Chem.* **2002**, *45*, 4119.
- Gilbert, K. M.; Boos, T. L.; Dersch, C. M.; Greiner, E.; Jacobson, A. E.; Lewis, D.; Matecka, D.; Prisinzano, T. E.; Zhang, Y.; Rothman, R. B.; Rice, K. C.; Venanzi, C. A. *Bioorg. Med. Chem.* **2007**, *15*, 1146.
- de Gregorio, C.; Kier, L. B.; Hall, L. H. *J. Comput. Aided Mol. Des.* **1998**, *12*, 557.
- Kier, L. B.; Hall, L. H. *Molecular Connectivity in Structure-Activity Analysis*; Research Studies Press, John Wiley and Sons: Chichester, UK, 1986.
- Kier, L. B.; Hall, L. H. *Molecular Structure Description: The Electrotopological State*; Academic Press: San Diego, 1999.
- Kier, L. B.; Hall, L. H. *Adv. Drug Res.* **1992**, *22*, 1.
- Kier, L. B.; Hall, L. H. *Pharm. Res.* **1990**, *7*, 801.
- Hall, L. H.; Mohnhey, B. K.; Kier, L. B. *J. Chem. Inf. Comput. Sci.* **1991**, *31*, 76.
- Hall, L. H.; Kier, L. B. *J. Math. Chem.* **1991**, *7*, 229.
- Kim, H.-J.; Cho, Y. S.; Koh, H. Y.; Kong, J. Y.; No, K. T.; Pae, A. N. *Bioorg. Med. Chem.* **2006**, *14*, 1454.
- Votano, J. R.; Parham, M.; Hall, L. M.; Hall, L. H.; Kier, L. B.; Oloff, S.; Tropsha, A. *J. Med. Chem.* **2006**, *49*, 7169.
- Varnek, A.; Kireeva, N.; Tetko, I.; Baskin, I.; Solov'ev, V. P. *J. Chem. Inf. Model.* **2007**, *47*, 1111.
- Hudson, B. D.; Hyde, R. M.; Rahr, E.; Wood, J. *Quant. Struct.-Act. Relat.* **1996**, *15*, 285.
- Kovatcheva, A.; Golbraikh, A.; Oloff, S.; Xiao, Y.-D.; Zheng, W.; Wolschann, P.; Buchbauer, G.; Tropsha, A. *J. Chem. Inf. Comput. Sci.* **2004**, *44*, 582.
- Available from Tripos Inc., St. Louis, MO.
- Kier, L. B.; Hall, L. H. *Molecular Connectivity in Chemistry and Drug Research*; Academic Press: New York, 1976.
- Kier, L. B. *Quant. Struct.-Act. Relat.* **1985**, *4*, 109.
- Hall, L. H.; Kier, L. B. *J. Chem. Inf. Comput. Sci.* **1995**, *35*, 1039.
- Clark, R. D.; Sprou, D. G.; Leonard, J. M. In *Rational Approaches to Drug Design: Proceedings of the 13th European Symposium on QSAR*; Høltje, H.-D., Sippl, W., Eds.; Prous Science, 2001; p 475.
- Cramer, R. D., III; Patterson, D. E.; Bunce, J. D. *J. Am. Chem. Soc.* **1988**, *110*, 5959.
- Whitley, D. C.; Ford, M. G.; Livingstone, D. J. *J. Chem. Inf. Comput. Sci.* **2000**, *40*, 1160.
- Lajiness, M. S. *Perspect. Drug Discovery Des.* **1997**, *718*, 65.
- Snarey, M.; Terrett, N. K.; Willett, P.; Wilton, D. J. *J. Mol. Graphics Modell.* **1997**, *15*, 372.
- Hoffman, B.; Cho, S. J.; Zheng, W.; Wyrick, S.; Nichols, D. E.; Mailman, R. B.; Tropsha, A. *J. Med. Chem.* **1999**, *42*, 3217.
- Tropsha, A.; Zheng, W. *Curr. Pharm. Des.* **2001**, *7*, 599.
- Xiao, Z.; Xiao, Y.-D.; Feng, J.; Golbraikh, A.; Tropsha, A.; Lee, K.-H. *J. Med. Chem.* **2002**, *45*, 2294.
- Oloff, S.; Mailman, R.; Tropsha, A. *J. Med. Chem.* **2005**, *48*, 7322.
- Itskowitz, P.; Tropsha, A. *J. Chem. Inf. Model.* **2005**, *45*, 777.
- Marini, F.; Roncaglioni, A.; Novič, M. *J. Chem. Inf. Model.* **2005**, *45*, 1507.
- Dutta, D.; Guha, R.; Wild, D.; Chen, T. *J. Chem. Inf. Model.* **2007**, *47*, 989.
- Scior, T.; Medina-Franco, J. L.; Do, Q.-T.; Martínez-Mayorga, K.; Yunes Rojas, J. A.; Bernard, P. *Curr. Med. Chem.* **2009**, *16*, 4297.
- Kim, K. H.; Greco, G.; Novellino, E. In *3D QSAR in Drug Design: Recent Advances*; Kubinyi, H., Folkers, G., Martin, Y. C., Eds.; Kluwer: Academic, Dordrecht, 1998; Vol. 3, p 257.
- Nicklaus, M. C.; Wang, S.; Driscoll, J. S.; Milne, G. W. *Bioorg. Med. Chem.* **1995**, *3*, 411.
- Veith, M.; Hirst, J. D.; Brooks, C. L., III. *J. Comput. Aided Mol. Des.* **1998**, *12*, 563.
- Boström, J.; Norrby, P.-O.; Liljefors, T. *J. Comput. Aided Mol. Des.* **1998**, *12*, 383.
- Debnath, A. K. *J. Med. Chem.* **1999**, *42*, 249.
- Perola, E.; Charifson, P. S. *J. Med. Chem.* **2004**, *47*, 2499.
- Guarnieri, F.; Weinstein, H. *J. Am. Chem. Soc.* **1996**, *118*, 5580.
- Hopfinger, A. J.; Tokarski, J. S. In *Practical Application of Computer-Aided Drug Design*; Charifson, P. S., Ed.; Marcel Dekker: New York, 1997; p 105.
- Barnett-Norris, J.; Guarnieri, F.; Hurst, D. P.; Reggio, P. H. *J. Med. Chem.* **1998**, *41*, 4861.
- Barnett-Norris, J.; Hurst, D. P.; Lynch, D. L.; Guarnieri, F.; Makriyanis, A.; Reggio, P. H. *J. Med. Chem.* **2002**, *45*, 3649.
- Greenidge, P. A.; Merette, S. A.; Beck, R.; Dodson, G.; Goodwin, C. A.; Scully, M. F.; Spencer, J.; Weiser, J.; Deadman, J. J. *J. Med. Chem.* **2003**, *46*, 1293.
- Bernard, D.; Coop, A.; MacKerell, A. D., Jr. *J. Am. Chem. Soc.* **2003**, *125*, 3101.
- Bernard, D.; Coop, A.; MacKerell, A. D., Jr. *J. Med. Chem.* **2005**, *48*, 7773.
- Golbraikh, A.; Tropsha, A. *J. Comput. Aided Mol. Des.* **2002**, *16*, 357.
- Golbraikh, A.; Shen, M.; Xiao, Y.-D.; Lee, K.-H.; Tropsha, A. *J. Comput. Aided Mol. Des.* **2003**, *17*, 241.
- Willett, P.; Winterman, V. *Quant. Struct.-Act. Relat.* **1986**, *5*, 18.
- Johnson, M. A. *J. Math. Chem.* **1989**, *3*, 117.
- Willett, P.; Winterman, V.; Bawden, D. *J. Chem. Inf. Comput. Sci.* **1986**, *26*, 36.

90. *Molecular Similarity in Drug Design*; Dean, P. M., Ed.; Blackie Academic & Professional: Glasgow, 1995.
91. Ferguson, A. M.; Patterson, D. E.; Garr, C. D.; Underiner, T. L. J. *Biomol. Screening* **1996**, *1*, 65.
92. Matter, H. J. *Med. Chem.* **1997**, *40*, 1219.
93. Wold, H. In *Multivariate Analysis*; Krishnaiah, P. R., Ed.; Academic Press: New York, 1966; p 391.
94. Wold, S.; Albano, C.; Dunn, W. J., III; Edlund, U.; Esbensen, K.; Geladi, P.; Hellberg, S.; Johansson, E.; Lindberg, W.; Sjöström, M. In *Chemometrics: Mathematics and Statistics in Chemistry*; Kowalski, B. R., Ed.; D. Reidel Publishing Company: Dordrecht, Holland, 1984.
95. Höskuldson, A. J. *Chemom.* **1988**, *2*, 211.
96. Frank, I. E.; Friedman, J. H. *Technometrics* **1993**, *35*, 109.
97. Clark, R. D. J. *Comput.-Aided Mol. Des* **2004**, *18*, 563.
98. Ding, Y.-S.; Fowler, J. S.; Volkow, N. D.; Dewey, S. L.; Wang, G.-J.; Logan, J.; Gatley, S. J.; Pappas, N. *Psychopharmacology* **1997**, *131*, 71.
99. Halgren, T. A. J. *Comput. Chem.* **1996**, *17*, 490.